



STATE RESEARCH CENTER OF RUSSIA
INSTITUTE FOR HIGH ENERGY PHYSICS

IHEP 97-58

S. Akimenko, G. Alekseev, Yu. Arestov, V. Belousov, B. Chuiko, V. Grishin, A. Derevschikov,
A. Davidenko, S. Erin, V. Kachanov, Yu. Kharlov, V. Khodyrev, A. Konstantinov,
V. Medvedev, Yu. Melnik, A. Meschanin, N. Minaev, V. Mochalov, A. Mysnik, A. Pavlinov,
D. Patalakha, A. Prudkoglyad, V. Rykalin, P. Semenov, V. Senko, **V. Solovianov**¹,
S. Stepushkin, O. Tsai, N. Ukhanov, A. Ufimtsev, A. Yakutin
(*Institute for High Energy Physics, Protvino*)

N. Borisov, E. Bunyatova, A. Kalinnikov, B. Khachaturov, M. Liburg, V. Matafonov,
A. Neganov, Yu. Plis, **Yu. Usov**²
(*Joint Institute for Nuclear Research, Dubna*)

Yu. Chestnov, O. Fedorov, P. Neustroev, V. Polyakov, **V. Vovchenko**³, A. Zhdanov
(*St. Petersburg Institute for Nuclear Physics, Gatchina*)

D. Crandell, **A.D. Krisch**⁴, A. Lin, R. Phelps, R. Raymond
(*University of Michigan, Ann Arbor, Michigan, USA*)

**A STUDY OF ONE-SPIN ASYMMETRIES
IN pp_{\uparrow} AND $\pi^{-}p_{\uparrow}$ INTERACTIONS
AT 70 AND 40 GEV/C**

(Proposal of experiment RAMPEX)

Collaboration Protvino-Dubna-Gatchina-Michigan

¹solovianov@mx.ihep.su

²usov@main2.jinr.dubna.su

³vovchenko@lnpi.spb.su

⁴krisch@miphys.physics.lsa.umich.edu

Abstract

Akimenko S. et al. A study of one-spin asymmetries in pp_{\uparrow} and $\pi^{-}p_{\uparrow}$ interactions at 70 and 40 GeV/c. (Proposal of experiment.): IHEP Preprint 97-58. – Protvino, 1997. – p. 39, figs. 22, tables 2, refs.: 53.

A Russian-AMerican Polarization EXperiment (RAMPEX) has been proposed to study one-spin asymmetries in the hadron production processes on polarized target $p(\pi^{-}) + p_{\uparrow} \rightarrow h + X$ and $p(\pi^{-}) + p_{\uparrow} \rightarrow h_1 + h_2 + X$ at the initial proton beam momentum 70 GeV/c and initial π^{-} beam momentum 40 GeV/c.

Аннотация

Акименко С. и др. Изучение односпиновых асимметрий в pp_{\uparrow} - и $\pi^{-}p_{\uparrow}$ -взаимодействиях при 70 и 40 ГэВ/с. (Предложение эксперимента.): Препринт ИФВЭ 97-58. – Протвино, 1997. – 39 с., 22 рис., 2 табл., библиогр.: 53.

Приведено описание русско-американского эксперимента РМПЭС для изучения односпиновых асимметрий в процессах адронного рождения на поляризованной мишени $p(\pi^{-}) + p_{\uparrow} \rightarrow h + X$ и $p(\pi^{-}) + p_{\uparrow} \rightarrow h_1 + h_2 + X$ при начальном импульсе протонного пучка 70 ГэВ/с и начальном импульсе пионного пучка 40 ГэВ/с.

Contents

1. Introduction	3
2. Experimental results	4
3. Physics motivation	7
3.1. Twist-3 in one-spin asymmetries	8
3.2. Twist-2 in one-spin asymmetries	9
3.3. Phenomenological models	11
3.4. Asymmetry $A_N(x_F, p_T)$ in the production of resonances	14
3.5. Flavor dependence of the asymmetry	14
3.6. Λ polarization measurements	15
4. Experimental setup	15
4.1. Beam	16
4.2. Polarized target	16
4.3. Magnetic spectrometer	16
4.4. Charged particle identification	17
4.5. Electromagnetic calorimeters	18
4.6. Trigger hodoscopes	19
4.7. Hadron calorimeter	20
5. Data acquisition system	21
5.1. Architecture of the system	21
5.2. Data flow	23
5.3. Rate estimations	23
6. Triggering	23
7. Estimates of cross sections and uncertainties	25

8. Status of equipment	31
8.1. Acceptance	31
8.2. Composition of the equipment	32
8.3. Equipment production and tuning	32
9. What shall we study – short formulation	33
References	34
10. Appendix A: Parton densities in a polarized nucleon	38
11. Appendix B: Factorization theorem with one spin	39

1. Introduction

Quantum chromodynamics as a model of strong interactions is commonly used in interpretation of experimental data. The most successful descriptions are those effects which correspond to the leading twist-2 contributions. These include collider data on hard photon and jet production at large p_T , on lepton pair production with large M etc. For some processes, the twist-4 corrections were determined in the $1/Q$ power series [QST91].

The whole class of *polarization* phenomena is also described in terms of twist-2 quark distributions arising in decomposition of non-perturbative proton matrix elements. First, $g_1(x, Q^2)$ is the quark distribution in longitudinally polarized protons. This function has been studied in deeply inelastic scattering of longitudinally polarized leptons (e, μ) on longitudinally polarized protons (deuterons) [DIS94]. There are theoretical papers which argue to measure another twist-2 quark distribution function, $h_1(x, Q^2)$ [RAL79],[ART90].

Compared to the leading twist terms, the higher twist contributions have been studied in few experiments (see for example ref. [AMM76]) since they are power corrections to the leading terms. However there are effects which are completely determined by the higher twists. They exist in reactions with unpolarized and with polarized particles as well. In this proposal, as a source of information about *twist-3* contributions we shall treat one-spin asymmetries in hard and semi-hard hadron production on polarized protons in reactions $pp_{\uparrow} \rightarrow h + X$. At the moment, there are no explicit model considerations which attribute the twist-3 one-spin asymmetry in pure hadron reactions to the chiral-odd twist-3 quark spin-dependent distribution $h_L(x)$.

We shall also study spin correlations in the double inclusive process $pp_{\uparrow} \rightarrow h_1 + h_2 + X$. We believe that they can be attributed to the convolution of the twist-2 quark distributions and quark fragmentation functions. This consideration will involve the chiral-odd twist-2 spin distribution $h_1(x)$.

Experiment RAMPEX – Russian-American Polarization EXperiment– will include a program of studies of the spin effects which have a clearly twist-3 origin and also effects of not-so-obviously twist-2 origin. A significant part of the investigations will be performed

for the first time. This program includes pp_{\uparrow} interactions at 70 GeV/c, and as an option $\pi^{-}p_{\uparrow}$ interactions at 40 GeV/c, at the Serpukhov accelerator.

2. Experimental results

Experimental measurements of one-spin asymmetries $A_N(x_F, p_T)$ in inclusive reactions at initial momenta of few GeV/c and higher have been performed since 1975, starting with the pioneering results of Dick [DIC75]. Later on, during 15 years, a number of experiments was performed at CERN and in Serpukhov (with polarized targets), in Argonne (with 6 GeV/c and 11.75 GeV/c polarized proton beams), in Brookhaven (with polarized proton beam at 13 and 18 GeV/c) and at Fermilab (with polarized beam of the maximum momentum 200 GeV/c). Measurements made in '70s and '80s are listed in [EXPAN]. They showed the presence of significant spin asymmetries for initial momenta in the range 6 to 24 GeV/c.

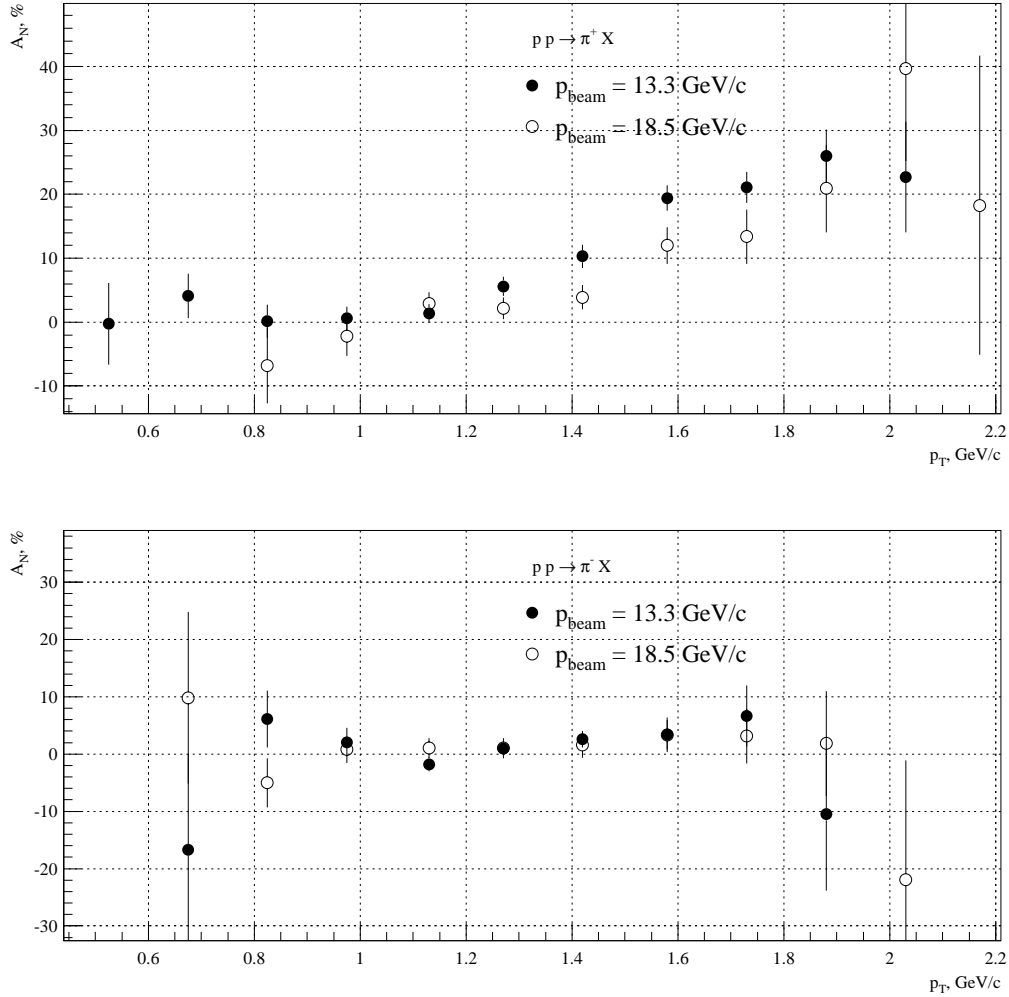


Fig. 1. Asymmetry $A_N(p_T)$ in reaction $p_{\uparrow} + p \rightarrow \pi^{\pm} + X$ at 13.3 and 18.5 GeV/c [SAR90].

The later results were published in 1990-92 and they covered the range of initial momenta from 13 to 200 GeV/c. In fig. 1 the dependence of asymmetry $A_N(p_T)$ on transverse momentum is shown for inclusive processes $p_{\uparrow} + p \rightarrow \pi^{\pm} + X$ at 13.3 and 18.5 GeV/c [SAR90]. The quantity $x_T = 2p_T/\sqrt{s}$ reaches very large values – 0.9 for π^+ and 0.8 for π^- production. The values of the π^- asymmetry are consistent with zero, and the π^+ asymmetry reaches 20% in the region of central production.

This behaviour of the asymmetries for π^+ and π^- production at $x_F = 0$ is confirmed by the results obtained in [BON90] at the same initial energies which are shown in fig. 2. The asymmetry values $A_N(x_F)$ at large x_F are also plotted.

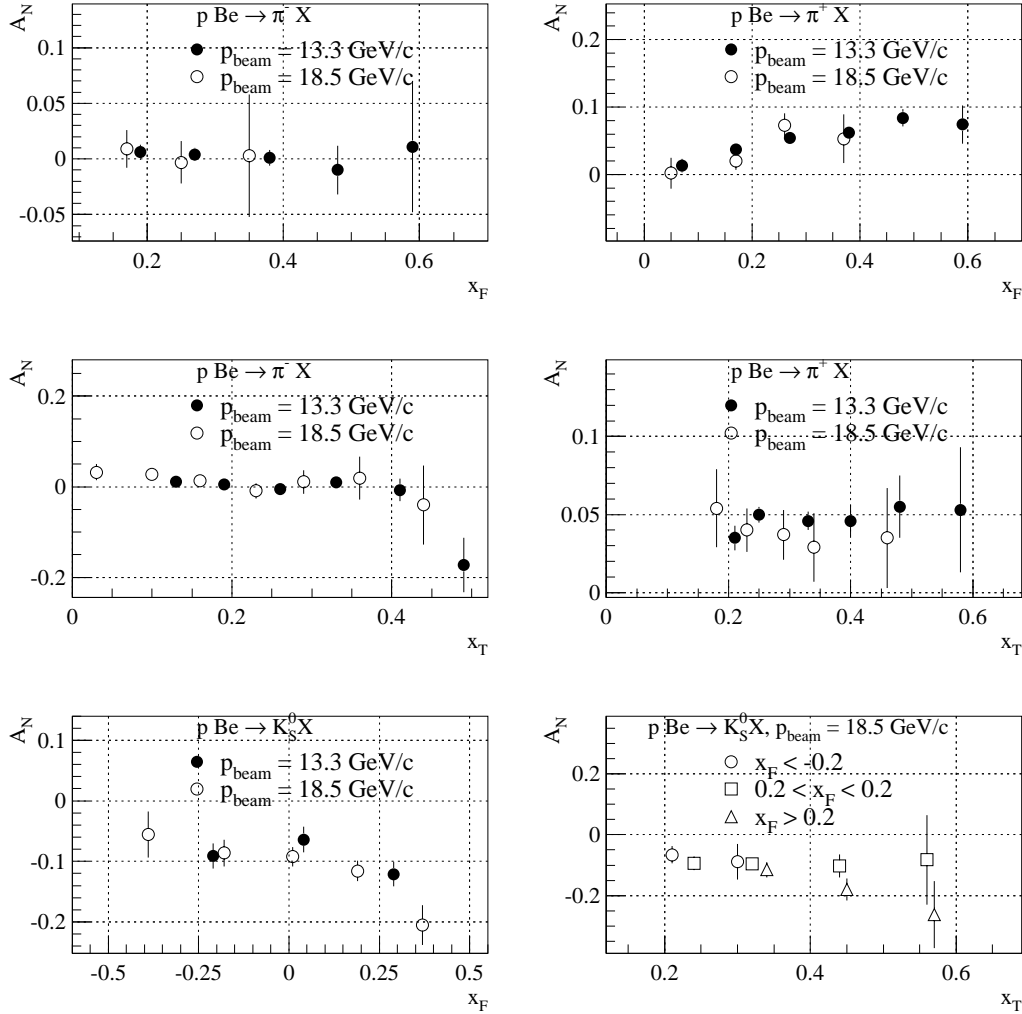


Fig. 2. Asymmetries $A_N(x_F)$ and $A_N(x_T)$ in reactions $p_{\uparrow} + p \rightarrow \pi^{\pm}, K_S^0 + X$ at 13.3 and 18.5 GeV/c [BON90].

For π^+ , the values of $A_N(x_F)$ are positive and vary from 0.05 to 0.10. Of special interest are the K_S^0 asymmetries in reaction $p_{\uparrow} + Be \rightarrow K_S^0 + X$, which are presented in this figure versus x_F and x_T . A_N is negative and it changes approximately from –0.05 to –0.25.

The Serpukhov results at 40 GeV/c are displayed in fig. 3a for the process $\pi^- + p_{\uparrow} \rightarrow \pi^0 + X$ at $p_T > 1.2 \text{ GeV}/c$ [APO90]. In the region $p_T \sim 2.5 \text{ GeV}/c$ the asymmetry achieves the maximum value $\sim 40\%$.

Figs. 3b,c present the measurements of the one-spin asymmetry in reactions with 200-GeV/c polarized proton beam $p_{\uparrow} + p \rightarrow \pi + X$ at large x_F (for π^+, π^-, π^0) and at $x_F=0$ (for π^0) taken from refs [ADA91a] and [ADA91b]. The x_F -dependences look impressive reaching the absolute values $\sim 40\%$ for charged pions. On the contrary, the asymmetry $A_N(p_T)$ in π^0 production at 90° in cms is consistent with zero in the wide p_T -interval from 1 to 4 GeV/c (fig. 3c).

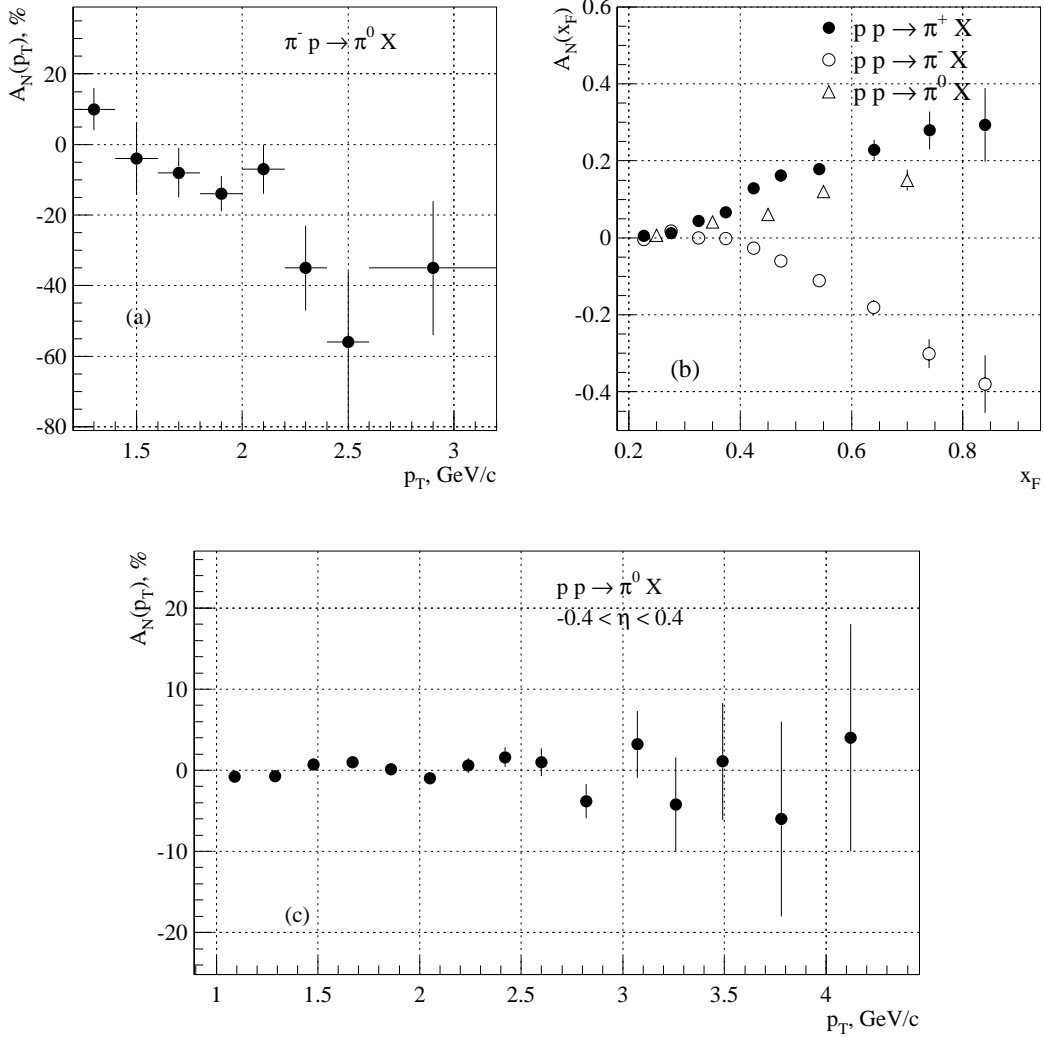


Fig. 3. a — Asymmetry $A_N(p_T)$ in reaction $\pi^- p_{\uparrow} \rightarrow \pi^0 + X$ at 40 GeV/c [APO90] ; b — E704 experiment at Fermilab: $A_N(x_F)$ in reaction $p_{\uparrow} + p \rightarrow \pi + X$ at $p_{lab} = 200 \text{ GeV}/c$ [ADA91a]; c — the same exp.: $A_N(p_T)$ for the central production of π^0 [ADA91b].

Analysing the whole set of experimental results which are available between beam momenta of 6 and 200 GeV/c, one can come up to the following conclusions:

- at any initial energy under study, the one-spin asymmetry can reach sizeable values;
- a serious enigma is the zero values of $A_N(p_T)$ in a very wide p_T -interval in E704 experiment at 200 GeV/c;
- the experimental measurements are rather mosaic, and mostly they cannot be compared;
- hence, from the quick review one can see the importance of a new experiment with a complex physical program which is able to give results on $A_N(x_F, p_T)$ for different particles and in different kinematical regions.

3. Physics motivation

Recent developments of theoretical representations of parton distributions in polarized protons have lead to new distribution functions and to their more adequate classification in chirality and twist (see for example [JAF91],[JIX92]). Normally the experimental community is familiar with the polarized parton densities $g_1(x)$ and $g_2(x)$, the first of which has been studied rather thoroughly. However the intrinsic nucleon structure is described also by other functions.

Although the best probing processes of the nucleon structure are photon processes either real (Compton, direct γ production) or virtual (DIS, Drell-Yan pairs), pure hadronic processes may contribute to the theory.

In this section the measurements of the one-spin asymmetries in hard and semi-hard hadron production processes are treated as a possible source of information on the new spin-dependent quark distributions $h_L(x)$ and $h_1(x)$, twist-3 and twist-2 respectively (see Appendix A). Actually in this experiment we shall measure the obviously-twist-3 asymmetries in single hadron production and we shall try to discover the more subtle twist-2 correlations in two-particle production processes. The definitions and simple introduction to h functions is given in Appendix A.

The well known studies of g_1 and g_2 distributions are based on the factorization formula which is strictly proved for deeply inelastic scattering with polarized leptons and protons. However this is not the case for hadron processes with one polarized proton. This problem is briefly discussed in Appendix B.

As follows from the factorization assumptions in Appendix B, the one-spin asymmetry can be determined by the integrand tensor convolution

$$\sigma_{\uparrow}(x_F, p_T) - \sigma_{\downarrow}(x_F, p_T) \sim h_L(x_b, Q) \otimes H(x_a, x_b, z). \quad (1)$$

Here $H(x_a, x_b, z)$ includes the quark distribution in unpolarized proton and the quark fragmentation function $D_{\pi/q}(z)$. This expression can be, in principle, applicable in a certain class of models for hard and semi-hard production processes [JAF91].

Our ability to contribute to the twist-3 studies depends on the knowledge - either theoretical or experimental - of the function H . Below we present the model approach [ANS95] in which a similar integrand was considered.

Theoretical problems relating to the chiral-odd distribution functions h_1 and h_L were discussed at the RAMPEX Round Table in Amsterdam, 1996 [ARE96]a.

3.1. Twist-3 in one-spin asymmetries

Contrary to the commonly accepted leading twist phenomenology in double-spin asymmetries, the twist-3 phenomenology of one-spin processes is not unique, and model approaches vary significantly. The pioneering study in this field was published in 1984 by A.Efremov and O.Teryaev [EFR84].

Twist-3 quark distributions. In early papers Efremov, Teryaev [EFR85] and Qiu, Sterman [QIS91] considered one-spin asymmetries A_N in processes with photons (Compton effect and direct gamma production):

$$\begin{aligned}\gamma N_\uparrow &\rightarrow \gamma + X \quad (\text{ET}), \\ p_\uparrow p &\rightarrow \gamma + X \quad (\text{QS}).\end{aligned}$$

They are proportional to the twist-3 proton matrix elements which are different in these studies due to the different twist-3 phenomenology.

Recently Efremov and collaborators [EFR95] obtained one-spin parton asymmetries in inclusive production of quark and gluons:

$$\begin{aligned}p_\uparrow + g &\rightarrow q + X, \\ p_\uparrow + g &\rightarrow g + X.\end{aligned}$$

These asymmetries are proportional to the quark-gluon correlation functions $b_A(y, x)$ and $b_V(y, x)$ which appear while factorizing the hadron process on the twist-3 level: $A_N \sim b_A(0, x) - b_V(0, x)$.

In hard and semi-hard hadron processes, a direct manifestation of the twist-3 quark densities are one-spin asymmetries in reactions with one transversely polarized proton in the initial state:

$$\begin{aligned}p + p_\uparrow &\rightarrow h + X, & 70 \text{ GeV}/c \\ \pi^- + p_\uparrow &\rightarrow h + X, & 40 \text{ GeV}/c.\end{aligned}\tag{2}$$

h denotes here charged and neutral π and K , protons, Λ and resonances, K_{890}^* и $\phi(1020)$ mainly. The asymmetry $A_N(x_F, p_T)$ in these reactions is fully determined by the twist-3 contribution since in perturbative QCD one-spin asymmetries are zero (in the limit of zero quark masses).

It is worthwhile saying that single inclusive reactions (2) can be used, in appropriate phenomenology, as a source of information about the chiral-odd distribution function h_L . In deep inelastic scattering there should be an additional hadron to be detected due to the chiral-odd nature of h functions. As to $h_L(x)$ in reactions (2), there is no model exploring this distribution function which is connected with the quark-gluon dynamics. However

as indicated in ref. [JAF91] it can be calculated in models with valence quarks, without dynamic gluons. One can say that the necessity of such model is inspired by the new experiment RAMPEX.

The main contribution to the cross sections of the processes (2) is normally given by the twist-2 terms, but the difference of the cross sections with opposite polarizations, i.e. the spin asymmetry, is determined by the twist-3 contribution (see formula (11)). The first considerations of the twist-3 terms in one-spin asymmetries were performed in ref. [EFR82]. The model references can be found in this section .

Expected measurements. The one-spin two-argument asymmetry $A_N(x_F, p_T)$ which will be measured in reactions (2) is defined as

$$A_N(x_F, p_T) = -\frac{1}{P} \frac{d\sigma_{\uparrow} - d\sigma_{\downarrow}}{d\sigma_{\uparrow} + d\sigma_{\downarrow}}. \quad (3)$$

Here P is a value of the target transverse polarization. The measurements will be performed in the regions of hard production of hadrons h (at $x_F = 0$) and of semi-hard production at large x_F . The hard processes are the most promising for extracting the twist-3 parton densities, since then the factorization formula (11) can be applied in the most unambiguous way. The model approaches in semi-hard region are more ambiguous. But in this case the asymmetry is also determined by the twist-3 terms if a lower transverse momentum limit is assumed at large x_F , $p_T \geq p_T^0$ (for example $p_T^0 = 1$ GeV/c). This helps to remove or to decrease the Regge poles' contribution to the asymmetry. Examples of the model considerations can be found in refs. [DOR91],[ART94].

In particular, we would like to clarify the problem of the value of $A_N(0, p_T)$ for π^0 hard production. The asymmetry measured in reaction $\pi^- p_{\uparrow} \rightarrow \pi^0 + X$ at 40 GeV/c was rather sizable at $p_T \approx 2.5$ GeV/c as well as at lower energies in pp_{\uparrow} interactions [SAR90],[BON90]. Measurements in $p_{\uparrow}p$ interactions at 200 GeV/c (FNAL, E704) resulted in zero values in the wide interval $p_T = 1 \div 3.8$ GeV/c [ADA91b]. We hope the 70-GeV/c results to give a fresh look at the behaviour of the asymmetry $A_N(0, p_T)$ in the energy interval from 40 to 200 GeV/c.

3.2. Twist-2 in one-spin asymmetries

Of twist-2 polarized quark distributions, only the function $g_1(x, Q^2)$ has been a subject to intensive experimental studies in DIS with longitudinally polarized leptons and protons (deutrons) [DIS94]. For $h_1(x)$, the chiral-odd twist-2 distribution function, there is no experimental information and no commonly used theoretical approach in hadron processes, though $h_1(x)$ is well understood as the 'transversity' distribution.

The one-spin asymmetry in hard processes with spatial parity conservation may exist at the leading twist-2 level only if a final state particle polarization is included in consideration. This is because the hard parton subprocess itself cannot give a measurable asymmetry even under summation of loop corrections. The final particle polarization may not be directly measured. Information about the spin state of a quark scattered in a subprocess can be inferred through detection of two hadrons produced by the quark.

In ref. [LEA93] Drell-Yan pair production is considered in the reaction $p_{\uparrow}p \rightarrow (\gamma^* \rightarrow e^+e^-) + X$ with the γ^* decay in the phase space $d\Omega^*$. This is equivalent to using the decay spin density matrix.

The Collins effect in hard and semi-hard regions. J.Collins suggested that the fragmentation function of the transversely polarized quark is expressed as

$$D_{\pi/q}(\mathbf{s}, z, \mathbf{p}_t) = D_{\pi/q}(z, p_t) \left(1 + \frac{\mathbf{s} \cdot (\mathbf{q} \times \mathbf{p})}{p_t} \mathcal{A} \right). \quad (4)$$

Here \mathbf{s} is polarization of a quark with momentum \mathbf{q} scattered in a hard subprocess and fragmented into pion of momentum $\mathbf{p} = (\mathbf{p}_l, \mathbf{p}_t)$ with the components parallel and perpendicular to the quark momentum.

The azimuthal differences arising from the formula (4) and resulting in left-right asymmetries were defined by Collins as a 'sheared jet asymmetry'[COL93],[COL94].

Expression (4) involves the azimuthal angle dependence in the plane transverse to the scattered quark direction. This dependence was explicitly explored in ref.[ART94] where the final state quark polarization is related to the twist-2 chiral-odd transversity distribution h_1 :

$$\mathbf{s} = \mathcal{R}(\mathbf{s}_{beam}) \frac{h_1(x, \mathbf{p}_t)}{f_q(x, \mathbf{p}_t)} \mathcal{D}_{NN}.$$

Here \mathcal{R} denotes the rotation around the normal to the quark scattering plane, $f_q(x, \mathbf{p}_t)$ is unpolarized quark distribution and \mathcal{D}_{NN} is the spin transfer in the subprocess.

Target fragmentation region. Similarly to the hard production, the spin correlations of the type (4) can be observed in the target fragmentation region. In this case \mathbf{q} is the direction of the incoming polarized target proton in cms. As the analysing power (left-right asymmetry) \mathcal{A} has a kinematic zero at $\mathbf{p}_t = 0$, the transverse momenta of the detected hadrons (pions) must be restricted, say, $p_t > 0.3$ GeV/c. The pion longitudinal momenta obey an appropriate condition, for example, $x_F < -0.3$.

One can use two leading particles with momenta \mathbf{p}_1 and \mathbf{p}_2 to define both the quark axis and the azimuthal angle. This leads to the correlations of type

$$\frac{\mathbf{s}(\mathbf{p}_1 \times \mathbf{p}_2)}{|\mathbf{p}_1 \times \mathbf{p}_2|}.$$

Two-pion correlations. As a probe of the function $h_1(x)$ we want to test the spin-particle correlations in the double inclusive process

$$p(\pi^-) + p_{\uparrow} \rightarrow h^{\pm} + \pi^{\circ} + X. \quad (5)$$

The produced hadrons have large transverse momenta in opposite directions in cms (back-to-back kinematics). As was noticed by Collins in [COL93], these reactions with transverse initial polarization have advantages compared to longitudinal polarization because

the latter requires three vectors (three particles in the final state) to determine *handedness* [NAC77], [EFR92], whereas two is enough for the transverse polarization.

In reaction (5), the charged hadron h^\pm is detected in the spectrometer arm for charged particles, and the neutral pion π^0 is to be reconstructed in the second arm which will consist of an electromagnetic calorimeter made of PbWO_4 crystals.

A different type of spin correlations arise in the reaction (5) and also in reaction

$$p(\pi^-) + p_\uparrow \rightarrow h^+ + h^- + X, \quad (6)$$

if both hadrons h^+ and h^- have kinematics of leading particles produced by a scattered quark. The total momentum of hh pair has a direction close to 90° in cms ($x_F^{hh} = 0$). In this case there is a correlation between hh plane, scattering plane and initial polarization [RSC92], [COL94]. These correlations are proportional to $h_1(x)H(z)$ that is a product of the twist-2 transversity distribution and fragmentation function. Similar measurements will be performed with semi-hard hh pairs produced at large x_F^{hh} .

By charged hadrons h^\pm , we mean π^\pm and K^\pm in the momentum intervals where they can be effectively identified by the Čerenkov counters (see subsection 4.4).

3.3. Phenomenological models

Apart from the models mentioned above, there is a number of other papers concerning the origin of one-spin asymmetries. Large-distance contributions are also studied in the phenomenology of parton orbital motion and in effective quark interactions with colored hadron remnants (see [ARE96]b, [TRO95], [BOR95]).

$q\bar{q}$ pair orbiting. In refs. [TRO95] a constituent quark model is considered where constituent quarks are surrounded with a cloud of quark-antiquark pairs. One-spin asymmetry arises due to the $q\bar{q}$ orbital momentum in the constituent quark structure. Predictions of this model for the one-spin asymmetry in inclusive production of π^+ , π^- , π^0 at 70 GeV/c are presented in fig. 4a (p_T -dependence) and in π^\pm production at 200 GeV/c in fig. 4b (x_F -dependence). At the initial momentum 70 GeV/c we are interested in the predicted values of the pion asymmetries are rather sizeable.

Valence quark orbiting. The 'Berliner model' of Meng and collaborators [BOR95] is based instead on the phenomenology of the valence quark orbiting. In fig. 4c predictions of the Berliner model are shown for inclusive pion production at 200 GeV/c in comparison with the Fermilab results.

Other large-distance effects. Large-distance interaction dynamics can be modelled by various means. Collins and Ladinsky in ref. [COL96] used the σ -model to describe the spin-dependent quark fragmentation to a two-pion state:

$$q \rightarrow \pi\pi + X.$$

They predict a non-zero dependence of fragmentation on the transverse spin on the level of twist-2 and show how the two-pion correlations reflect the quark spin. Although being a crude qualitative estimation this model is interesting as well as other pioneer works describing the twist-2 effects of the transverse polarization of initial quarks.

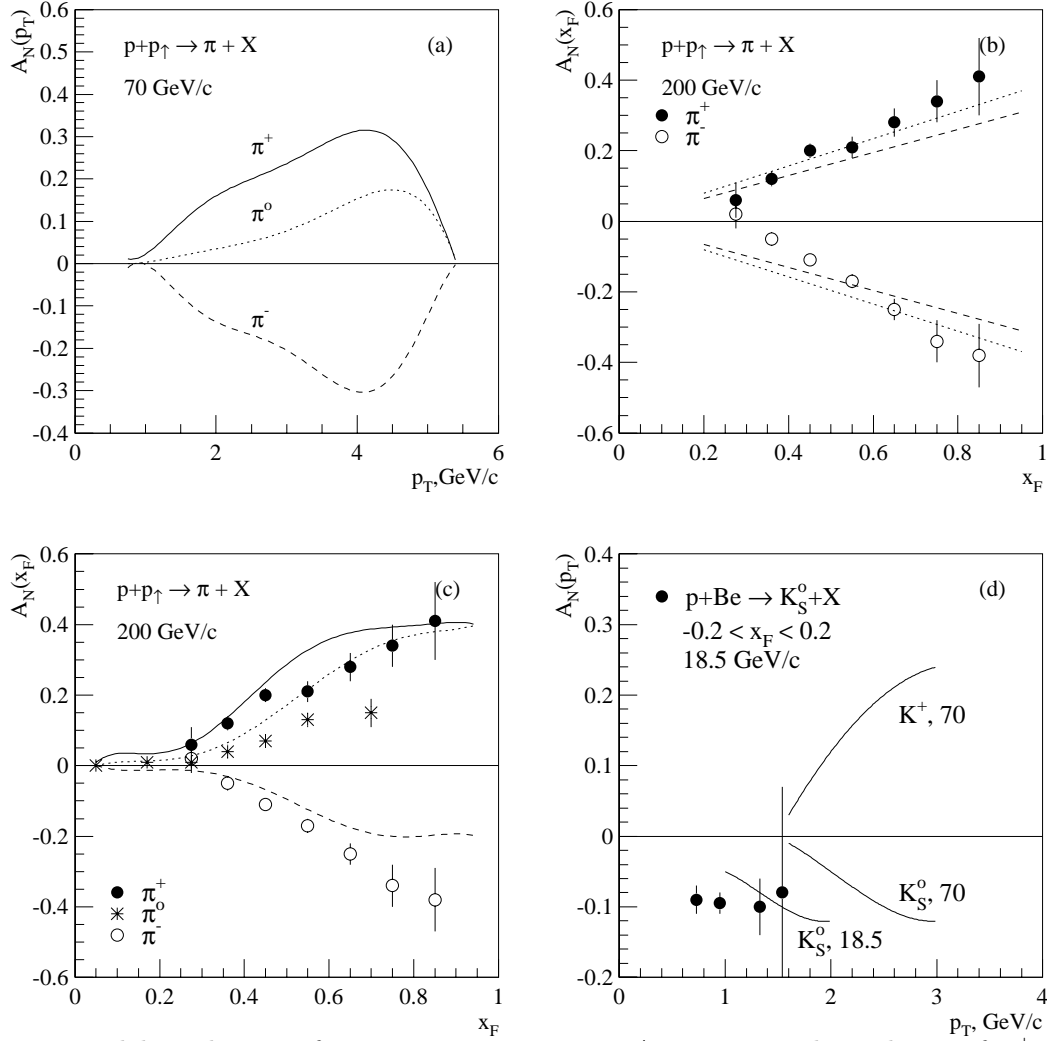


Fig. 4. Model predictions for one-spin asymmetry A_N : a — p_T -dependence of π^\pm, π^0 asymmetries at 70 GeV/c in the U -matrix model including the $q\bar{q}$ orbital motion [TRO95]; b — x_F -dependence of the π^\pm asymmetry at 200 GeV/c in the same model, different curves correspond to different model parameters; c — pion asymmetries at 200 GeV/c in the Berlin model with orbiting valence quarks [BOR95]; d — asymmetries of K^+ and K_S^0 -mesons in the model with quark spin flip in colored hadron remnant [ARE96]b.

At large distance, the spin of a scattered quark can be flipped in interactions with the colored field of the hadron remainder. This can be interpreted differently. In ref. [RYS90], quark chromomagnetic moment χ_q interacted with color field tube resulting in a model parameter χ_q . Else, in ref. [ARE96]b the quark spin flip was explained by a soft gluon radiation (absorption) in the quark fragmentation resulting in increasing p_T -dependence of the asymmetry. In fig. 4d the model predictions for $A_N(p_T)$ [ARE96]b are plotted in K -meson inclusive production at 70 GeV/c.

Intrinsic k_T . An application of intrinsic partonic k_T -structure of polarized protons to the one-spin asymmetry problem was performed by Sivers in [SIV90]. This idea was further developed by Anselmino and collaborators [ANS95]. They argue that indications

to the T -invariance violation in this approach are true only in the leading twist approximation. Based on the twist-3 contribution the expression for the one-spin asymmetry in the model of [ANS95] is

$$A_N d\sigma = \sum \int dx_a dx_b d^2 \mathbf{k}_{T_a} I_{+-}^{a/p}(x_a, \mathbf{k}_{T_a}) f_{b/p}(x_b) [d\hat{\sigma}/d\hat{t}(\mathbf{k}_{T_a})] D_{\pi/c}(z)/z.$$

All quantities in this equation are either theoretically or experimentally known, with the exception of the new function $I_{+-}^{a/p}(x_a, \mathbf{k}_{T_a})$. This function reflects the non-perturbative proton structure and includes conceptually the twist-3 quark distributions. Being appropriately parametrized, say as

$$I_{+-}(x, \mathbf{k}_T) = Nx^\alpha(1-x)^\beta g(k_T)$$

with the Gaussian $g(k_T)$, the function $I_{+-}(x, \mathbf{k}_T)$ can be extracted from experiment.

Model predictions for $A_N(x_F)$ at 70 GeV/c [ANS96] are shown in fig. 5a.

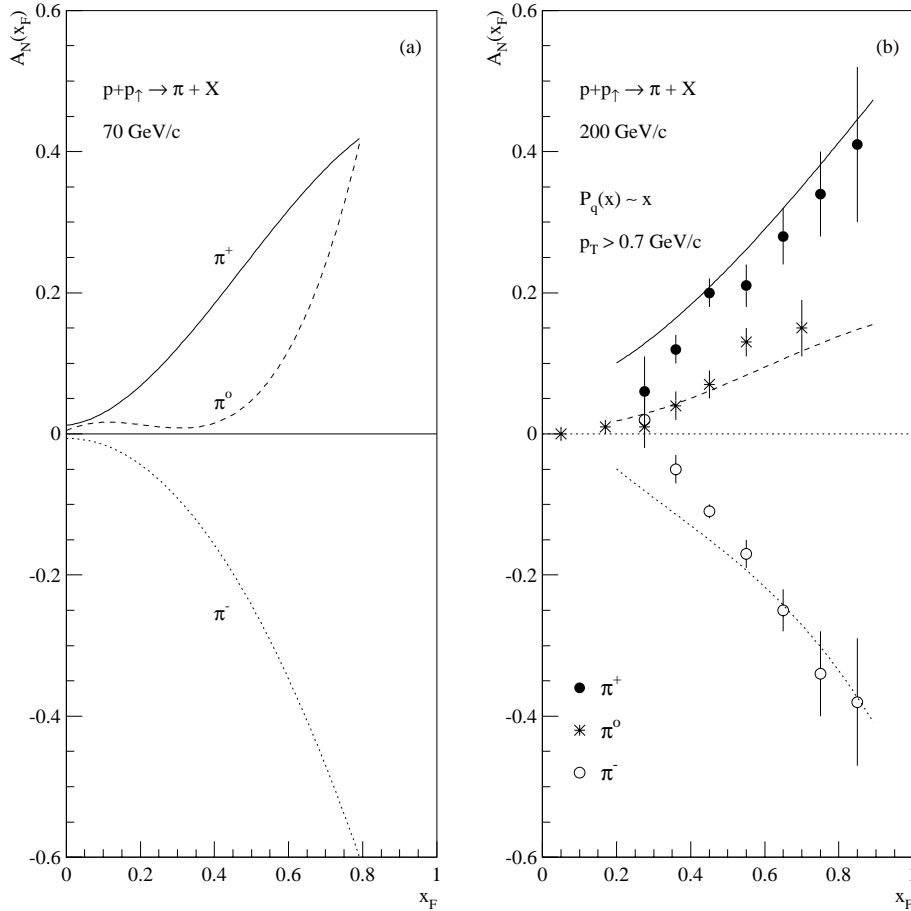


Fig. 5. The large- x_F behaviour of the one-spin asymmetry A_N : a — predictions of the model [ANS95] for 70 GeV/c made for RAMPEX due to the courtesy of Mauro Anselmino and Francesco Murgia; b — comparison of one of the model curves from [ART94] and the E704 data at 200 GeV/c.

Direct implementation of $h_1(x)$. Using the formula (4) X.Artru and collaborators attempted to include directly the twist-2 quark transversity distribution $h_1(x)$ in the integrand expressing the origin of the A_N [ART94]. After a number of subsequent simplifications, the large- x_F predictions for A_N at 200 GeV/c were obtained. They are presented in fig. 5b in comparison with the experimental data.

3.4. Asymmetry $A_N(x_F, p_T)$ in the production of resonances

Since a major part of hadrons is produced from resonances, measurements of one-spin asymmetry in resonance hard production will give more direct information about the twist-3 contributions. However a problem of background asymmetry seems to be a serious one. The reactions under study will be

$$\begin{aligned} p(\pi^-) + p_{\uparrow} &\rightarrow (K_{890}^* \text{ or } \bar{K}_{890}^*) + X, \\ p(\pi^-) + p_{\uparrow} &\rightarrow \phi(1020) + X \end{aligned} \quad (7)$$

with the decays $K_{890}^* \rightarrow K\pi$ and $\phi \rightarrow K^+K^-$. The distributions in invariant mass of detected pairs $K\pi$ and KK at $x_F = 0$ are shown in fig. 6. The ratio signal/background seems to be reasonable and it allows us to hope that the asymmetries of resonances can be measured.

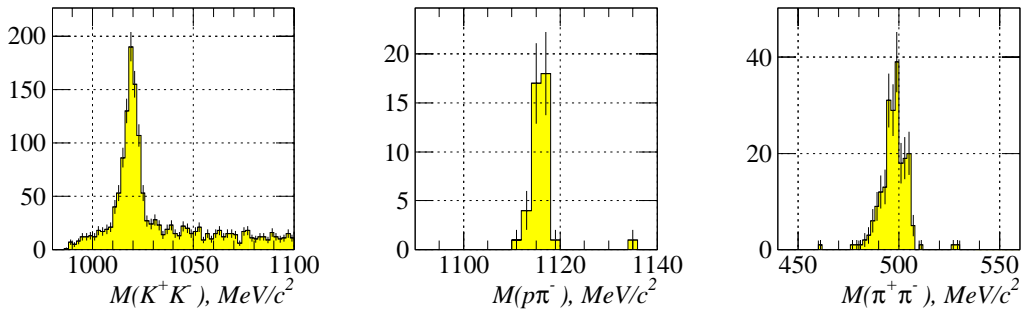


Fig. 6. Distributions in invariant mass of detected pairs of the charged particles.

3.5. Flavor dependence of the asymmetry

A comparison of polarization effects in inclusive production of particles with various quark content is of special interest. We therefore want to compare one-spin asymmetries in the following reactions:

$$\begin{aligned} p(\pi^-) + p_{\uparrow} &\rightarrow \pi^0 + X && (d\bar{d}) \\ &\rightarrow K_s^0 + X && (d\bar{s} + \bar{d}s) \\ p(\pi^-) + p_{\uparrow} &\rightarrow \pi^+ + X && (u\bar{d}) \\ &\rightarrow K^+ + X && (u\bar{s}) \\ p(\pi^-) + p_{\uparrow} &\rightarrow \pi^- + X && (d\bar{u}) \\ &\rightarrow K^- + X && (s\bar{u}). \end{aligned}$$

The one-spin asymmetry on the subprocess level which originates from perturbative QCD is proportional to the mass of the polarized quark. The masses of u, d quarks are negligibly small, and it is commonly believed that the strange quarks in polarized proton are weakly polarized.

On the contrary, the one-spin asymmetry originating from the twist-3 contributions is proportional to the mass parameter μ_{hadr} [EFR84], [EFR85] due to the long-distance interactions. As the fragmentation properties may differ for pions and kaons, the effective size of this region, $\sim 1/\mu_{\text{hadr}}$, may also vary, thus resulting in a flavor dependence of the one-spin asymmetries.

3.6. Λ polarization measurements

The decaying Λ -hyperons are good self-analysing polarization tools. The measurement of the final-state Λ polarization in the reaction

$$p + p_{\uparrow} \rightarrow \Lambda_{\uparrow} + X \quad (8)$$

will allow the study of the correlation parameter D_{NN} which is called polarization transfer coefficient and is defined as

$$D_{NN} = \frac{1}{P_T} \frac{N_{\uparrow\uparrow} + N_{\downarrow\downarrow} - N_{\uparrow\downarrow} - N_{\downarrow\uparrow}}{N_{\uparrow\uparrow} + N_{\downarrow\downarrow} + N_{\uparrow\downarrow} + N_{\downarrow\uparrow}}.$$

Here the vertical arrows in subscripts indicate the transverse polarization of the target and produced Λ .

The maximum values of the polarization transfer are expected in the target fragmentation region according to the naive quark-diquark representation of the polarized target proton.

The recent E704 measurements at Fermilab [PEN95] give evidence for a sizeable and positive value of D_{NN} .

4. Experimental setup

A brief description of RAMPEX can be found in [ARE97]. The full version of the experimental setup includes two arms (fig. 7).

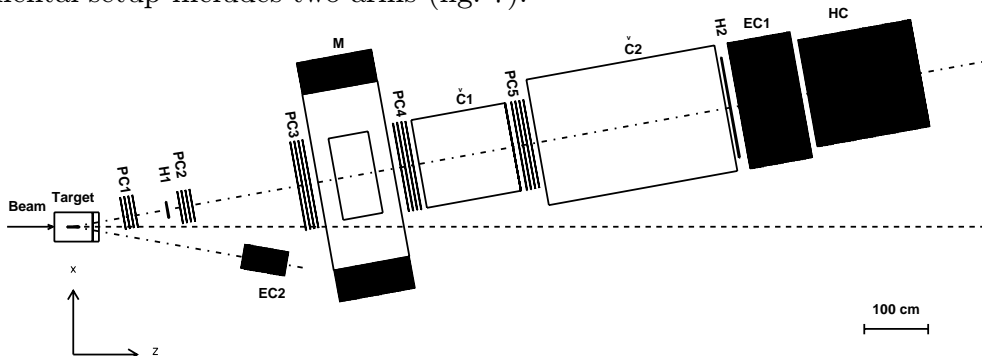


Fig. 7. Layout of experimental setup RAMPEX: PC1–PC5 — blocks of proportional chambers, M — analysing magnet, H1, H2 — trigger hodoscopes, Č1, Č2 — threshold Čerenkov counters, EC1, EC2 — electromagnetic calorimeters, HC — hadron calorimeter.

One arm consists of the magnet spectrometer, two Čerenkov counters Č1, Č2 to identify charged particles, an electromagnetic calorimeter EC1 and a hadron calorimeter HC. The magnet spectrometer consists of the magnet M and five proportional chambers PC1-PC5. In fig. 7 this arm makes an angle of 9° with the beam line corresponding to 90° in cms. This arm will be also rotated to a smaller angle close to 0° to detect particles with large x_F and to a larger angle to detect particles with negative x_F . Numerical estimations of acceptances and efficiencies show that the angle values near 80 and 300 mrad are optimal for these measurements.

The second arm of the setup consists only of the fine-granulated electromagnetic calorimeter EC2 which is placed symmetrically to the beam line and makes angle -9° or smaller.

4.1. Beam

Existing equipment of the 14th channel allows use of a 40 GeV/c π^- beam with the 1.8% K^- and 0.3% \bar{p} contamination [BRU75] and the 70 GeV/c unpolarized proton beam extracted directly from the accelerator with a bent Si crystal [ASE93]. We assume the pion/proton beam intensity of $5 \cdot 10^6$ in a 1-second spill with a 9-second interval between spills. The size of the pion beam is characterized by the values $\Delta_x = \pm 8$ mm, $\Delta_y = \pm 6$ mm with ± 2.5 mrad and ± 1.5 mrad angular divergences, horizontal and vertical respectively. The momentum uncertainty of the pion beam is defined by $\delta p/p = \pm 2.5\%$ [BRU75].

The transverse size of the proton beam is smaller by a factor of 2, and the angular divergence is smaller than ± 0.3 mrad [ASE93].

4.2. Polarized target

The parameters of the polarized target was published in ref. [BOR76]. Propane-diol $C_3H_8O_2$ fills a cavity 20 mm in diameter and 200 mm in length. The polarization of the hydrogen nuclei is about 80% on average. The dilution factor depends on a type of detected particle and kinematics, and varies between about 6 to 10. The target contains $9.3 \cdot 10^{24}$ nucleons/cm². The luminosity of the experiment is estimated as $\mathcal{L} \sim 5 \cdot 10^{31}$ cm⁻²spill⁻¹.

4.3. Magnetic spectrometer

The magnetic spectrometer was designed for the NEPTUN project. It includes the analysing magnet M and 5 blocks of multiwire proportional chambers PC1 – PC5. Each block contains four coordinate planes: orthogonal x and y planes and also u and v planes which are inclined to $\pm 10^\circ$ with respect to y axis. Fig. 7 represents an option with the spectrometer axis making an angle of 9° with the beam line. This position corresponds to 90° in cms at the initial momentum $p_{\text{beam}} = 70$ GeV/c to detect the hard production of hadrons.

The magnet M has the aperture 1.3×0.62 m² and the length 0.63 m. The integral of the magnetic field is 1.0 Tm. The magnet center is placed 4.5 m from the target center.

Two blocks of proportional chambers PC1 and PC2 with the transverse size $530 \times 384 \text{ mm}^2$ are located at distances 0.9 and 2 m from the target center, respectively. Three blocks of chambers PC3 – PC5 of size $1422 \times 898 \text{ m}^2$ are placed at the distances 3.7, 5.2 and 7.2 m from the target. The coordinate wires are stretched with a spacing of 2 mm in all planes.

The tracking system will allow us to measure charged particle momenta with an accuracy $\Delta p/p = 1.7 \cdot 10^{-3}p + 2 \cdot 10^{-3}$ and to reconstruct the straight-line track $x = x_0 + a_x z$ with an accuracy $\delta x_0 = 2 \text{ mm}$, $\delta a_x = 8.8 \cdot 10^{-4}$. In fig. 8 the dependence Δp vs p is shown.

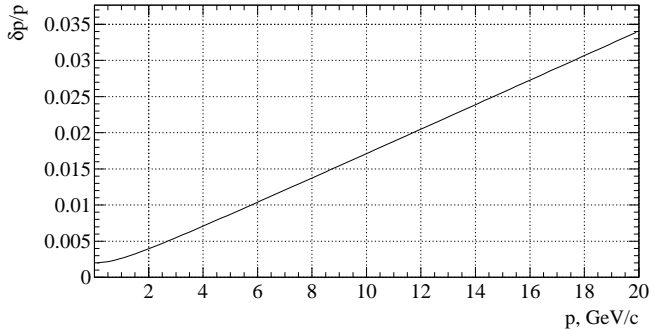


Fig. 8. Accuracy in momentum measurements of charged π , K , p .

4.4. Charged particle identification

Particle types for π , K , p and \bar{p} are determined with the help of two threshold multi-channel Čerenkov counters Č1 and Č2 which are placed downstream of the magnetic spectrometer. The counter Č1 has 8 channels (4×2) and it is filled with freon-12 at 1 atm. The 16-channel counter Č2 (8×2) is filled with the nitrogen also at 1 atm. The counters are designed to allow detection of multiple charged signals. Combinations of two counters can identify π^\pm with momenta $3.1 \div 20 \text{ GeV}/c$, and K^\pm and p^\pm from 10 to 20 GeV/c.

The aperture and the length of Č1 are $1.2 \times 0.9 \text{ m}^2$ and 1.5 m. The same characteristics for Č2 are $1.6 \times 0.88 \text{ m}^2$ and 3.0 m.

The counter mirrors are spherical, made of glass with 2 mm thick. The mirrors in counters Č1 and Č2 have sizes $30 \times 50 \text{ cm}^2$ and $25 \times 50 \text{ cm}^2$ respectively. The mirrors are covered with a reflecting layer to obtain maximum light reflection in the region of the PMT sensitivity. At the focus of each mirror a photo-multiplier tube PMT-174, with a photocathode 100 mm in diameter, is placed. Estimations show that this photocathode diameter results in the light collection efficiency of at least 50% [ALE94]. Quantum efficiency of the photocathode at the wave length 400 nm is about 25%.

Calculations of the counters' efficiencies are shown in fig. 9a,b. The number of photoelectrons is given assuming 90% light collection efficiency.

While identifying charged kaons, the pion contamination arises from the inefficiency of the counter Č2. The contamination can be estimated since the ratio of π 's to K 's is experimentally known. The results are plotted in fig. 9c under reasonable assumption of the 45% light collection efficiency. As is seen, at 11 GeV/c the pion contamination in kaons is less than 1%. Since the probability of the simultaneous misidentifications of the counters Č1 and Č2 is negligibly small, the major part of contamination in protons and antiprotons is due to charged kaons because of the inefficiency of the counter Č1. The relevant calculations are presented in fig. 9d. From this it follows that at 12 GeV/c the

contamination is about 10% and it decreases quickly with increasing particle momentum (down to 1% at 14 GeV/c).

Errors in particle identification may also arise from false counter signals from energetic δ -electrons. Estimations show that the number of the false signals is not greater than 0.003 per charged particle.

13/06/95 13.56

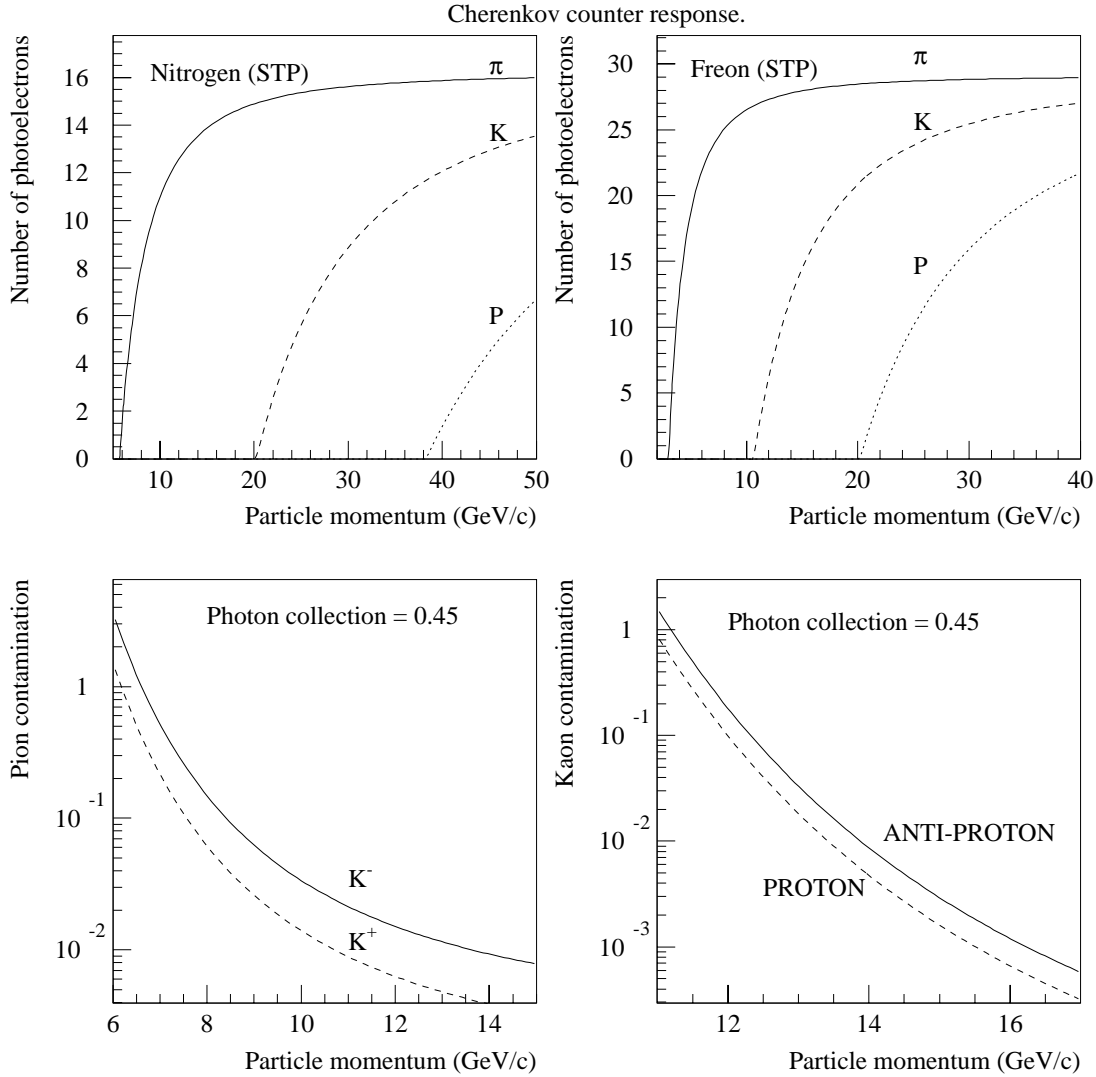


Fig. 9. Calculated properties of the Čerenkov counters.

4.5. Electromagnetic calorimeters

The calorimeter EC1 is being constructed of modules which were designed for the backward and forward γ -detectors of experimental setup NEPTUN. Both types of the modules are made as the Pb+Sci sandwich with layers which are perpendicular to the

direction of the detected particles. The light guide to the PMT is made by the longitudinal wave-length shifters (WLS).

The 1st-type cells. The transverse size of these cells is 76mm×76mm. The thickness of each layer of Pb and Sci is 2.5 mm and 5 mm respectively. The total length is about 20 radiation lengths, $20X_0$. The design includes use of an additional WLS in each cell to collect light only at the depth of the predicted electromagnetic shower maximum. Information about the longitudinal development of a shower will improve discrimination of the hadron background. The energy resolution for electrons follows the formula

$$\frac{\sigma_E}{E} \approx \frac{9\%}{\sqrt{E}} + 0,5\%.$$

The coordinate resolution is $\sigma_x \approx 1 \div 2$ mm at 26 GeV.

The 2nd-type cells. The transverse size of these cells is 38×38 mm. The thickness of each layer of Pb and Sci is 3 mm and 5 mm respectively. The length is about 22 radiation lengths, $22X_0$. The test of the prototype showed energy resolution

$$\frac{\sigma_E}{E} \approx \frac{9\%}{\sqrt{E}} + a,$$

where the constant a is much less than 0.01. The coordinate resolution is $\sigma_x \approx 1$ mm.

The center of calorimeter EC1 consists of a matrix 40×24 of the second-type cells of size 38×38 mm². The construction formula is 60 supermodules each consisting of 16 cells, thus giving totally 960 channels. The peripheral part of EC1 is formed by 144 first-type cells of size 76×76 mm². The construction formula is 36 supermodules, each of which contains 4 cells, resulting a total of 144 cells.

The calorimeter EC2 is placed much closer to the target than EC1. This requires a more compact design in comparison with lead glass or with sandwich calorimeters. As a radiator, we shall use heavy scintillating monocrystals of PbWO₄ [BUY94]. The small values of the radiation length ($X_0=9$ mm) and the Moliere radius ($R_M=20$ mm) allow reduction of the distance from the target by a factor of 2 without losing efficiency in π^0 reconstruction or angular resolution for single gammas and electrons. Another advantage of this detector is the high energy resolution:

$$\frac{\sigma_E}{E} \approx \frac{3\%}{\sqrt{E}} + 0,5\%.$$

4.6. Trigger hodoscopes

The scintillator hodoscopes H1 and H2 are used for fast estimation of particle momenta. The hodoscopes have two planes each. H1 has transverse size 260 × 130 mm² and consists of 26 × 13 channels. The transverse size of H2 is 1600 × 1100 mm² and it consists of 32 × 22 channels.

4.7. Hadron calorimeter

The hadron calorimeter consists of modules designed for the NEPTUN experiment at the internal beam of UNK [ALE92]. It will be used to detect K_L^0 and neutrons and also as an element of the trigger system. The hadron calorimeter of compensating type is a matrix of 18×12 modules (216 channels total). Each module is constructed as a sandwich Pb+Sci with the light collection in wave-length shifters (WLS). The ratio of the Pb and Sci thickness is equal to 4:1 and it has been chosen for compensation. The transverse size of a module is $10\text{cm} \times 10\text{cm}$, the length is equal to ≈ 6.5 nuclear lengths. The signal spectra of the hadron calorimeter produced by protons, pions and electrons are shown in fig. 10.

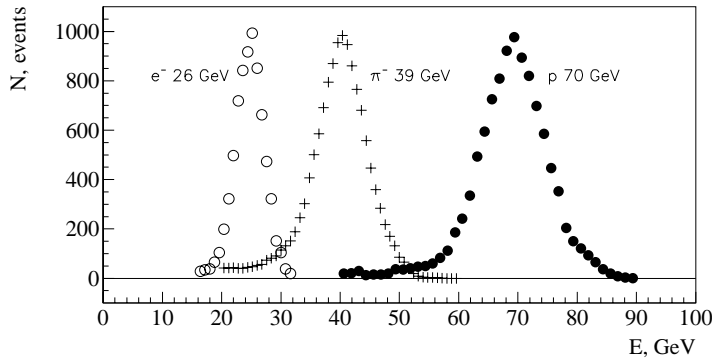


Fig. 10. The signal spectra of the hadron calorimeter when testing by the protons, π -mesons and electrons with the energies 70, 39 and 26.6 GeV respectively.

Compensation requires equality of signals from hadron and electromagnetic showers. It is an important property of HC resulting in high quality hadron calorimetry. Parameters of non-compensated HCs becomes much worse with increasing energy (fig. 11). They have low energy resolution and suffer from non-linearity of the energy scale.

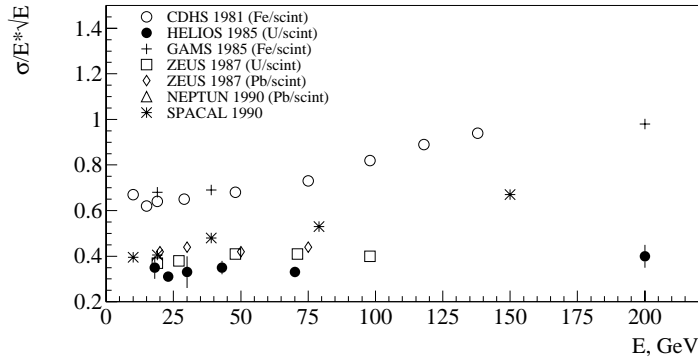


Fig. 11. Energy resolution of some known hadron calorimeters.

For HC, it has been measured in beam tests that the ratio of electron to hadron signals is equal to $e/h = 1.01 \pm 0.03$ (fig. 10). The energy resolution is

$$\frac{\sigma_E}{E} \approx \frac{57\%}{\sqrt{E}}.$$

Coordinate resolution has been measured as $\sigma_x \sim 5$ mm for the 40-GeV hadrons.

5. Data acquisition system

5.1. Architecture of the system

The Data Acquisition system (DAQ) and the program trigger (PT) use a heterogeneous distributed computer system based on various bus standards: MISS (IHEP), CAMAC, Q-BUS, VME and ETHERNET. Such variety of the bus standards originates from different types of the front-end electronics. DAQ and PT are globally controlled with the processing utilities under the real-time operational system OS9. A schematic layout of DAQ, PT and on-line data analysis is shown in fig. 12.

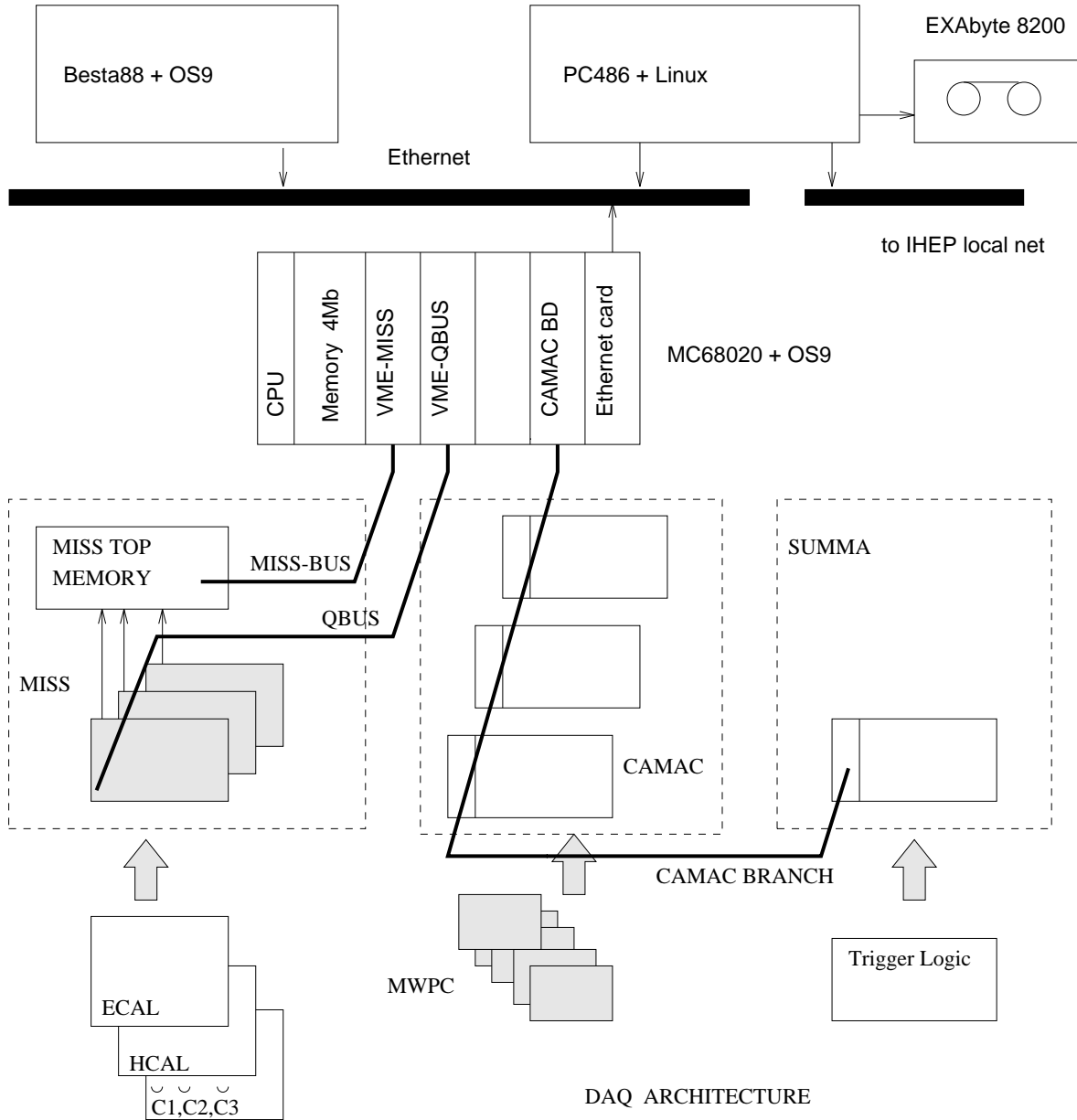
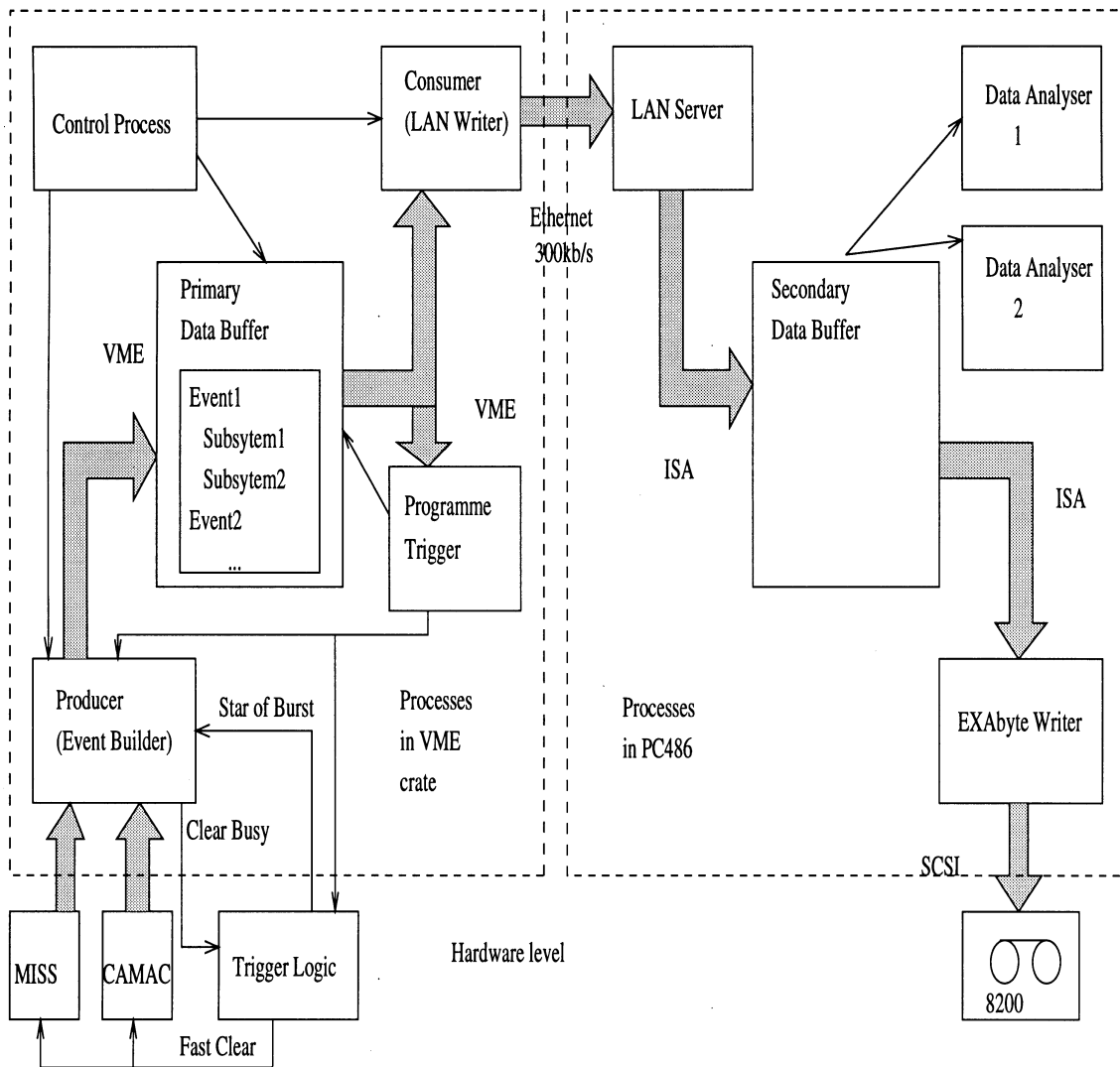


Fig. 12. DAQ Architecture.

The VME-MISS adapter provides a fast data channel from a buffer memory of a subsystem based on the MISS standard. QBus is needed for a slow control and the MISS electronics monitoring. A VME-QBus interface allows this control from the main VME crate.

Another VME crate is included in the BESTA88 workstation hardware. The programmable trigger is realized as processes under OS9 control in one or more processors (MC68020) of the main VME crate.

To be recorded in the archive storage and/or to be handled on-line, the formatted data are examined by the program trigger and then they are pumped through the Ethernet bus to PC486. The latter works under the operating system Linux (PC Unix clone). EXAbyte-8200 is used as the data storage device.



DATA FLOW

Fig. 13. Data Flow Diagram.

5.2. Data flow

A block-scheme of the DAQ processor is shown in fig. 13. The main process of the data read out (Producer) which performs also the functions of Event Builder, is interrupted by the Start of Burst (SoB) signal and then polls the MISS interface. The data is read into the Primary Data Buffer being formatted in the frame of events and subsystems. The data consumers are PT and LAN writer, the latter sending data through Ethernet.

Control process allows the DAQ user to control the data collection and informs of errors. OS9 supplies powerful interprocess communication, providing stability to the multiprocess system and effective monitoring of the global data buffer. The data flow structure in the on-line computer is organized around the Secondary Data Buffer. The Buffer distributes data among the various consumers assigning a high priority to the EXAbyte Writer to avoid the loss of data.

5.3. Rate estimations

Amplitude analysis is performed with ADC modules LE-61 (MISS) having the conversion time $50 \mu\text{s}$ and the conversion frequency 80 MHz (12 bits). Using the autonomic controller LE-22 to read out ADC and to send data, one has a mean data transfer speed 4 Mb/s or two 16-bits words per μs . Assuming the average total number of initialized cells per event to be equal to 40 in the electromagnetic calorimeter and 50 in the hadron calorimeter, the total amount of information from the MISS subsystem is equal to about 100 16-bit words. This includes 10 words which are read out per event from the hodoscopes and Čerenkov counters.

Thus the total time per event in the MISS subsystem is equal to $90/2 + 50 = 95 \mu\text{s}$. 10 words from hodoscopes and counters are read out within the LE-61 conversion time.

A serial 8-bit bus with the 1 MHz clock is used to read out MWPC. The controller made in the CAMAC standard is capable for cluster coding and zero compression. The possibility is reserved of using one controller for each chamber, that is to read out all chambers in parallel. The conversion time of the controller for an event with three clusters is $(4 \mu\text{s} \times 12 \text{ clusters} + 1 \mu\text{s} \times (700 \text{ wires} \times 4)/8 \text{ bits}) \approx 400 \mu\text{s}$. The time needed to read out this information thru the CAMAC dataway is equal to $1.5 \mu\text{s} \times 12 \times 5 \text{ chambers} \approx 90 \mu\text{s}$. The total time is equal to $\sim 500 \mu\text{s}$.

$5 \mu\text{s}$ after digitization of the calorimetric signals starts, the program trigger is switched on to process initially the information from the hodoscopes and Čerenkov counters and, after about $95 \mu\text{s}$, the calorimetric information. The Program Trigger decision time is up to $400 \mu\text{s}$. Thus in this sample event the maximum DAQ data flow is ~ 2000 events per burst (1 sec/500 μs), with the event size $\sim 0.5 \text{ Kb}$ or 1 Mb per burst. This is less than the EXAbyte upper limit of data recording ($250 \text{ Kb/sec} \times 8 \text{ sec} = 2 \text{ Mb}$).

6. Triggering

Principal scheme. The zero level trigger is arranged to strobe information from the trigger hodoscopes. The decision 'YES' is formed by the beam logic when a beam particle

of the required type is detected by the beam hodoscopes and strikes the active zone of the polarized target (beam flux T_0). The simplest first level trigger for the charged arm of the spectrometer is a coincidence of signals from the trigger hodoscopes $H1_y$ and $H2_y$. The estimations show that this trigger will allow a reduction of the data flow from the spectrometer by a factor of 10 or more.

To perform a fast kinematic selection of events with the trigger hodoscopes H1, H2 and the multichannel threshold Čerenkov counters Č1 and Č2, the electronic system with programmable logic developed in PNPI (Gatchina) will be used. The trigger logic scheme is shown in fig. 14. It consists of 32-channel discriminator-coders, 4-coordinate programmable logic and a module for the logic analysis. The dead time of the system is 20 ns, the signal delay is not more than 100 ns.

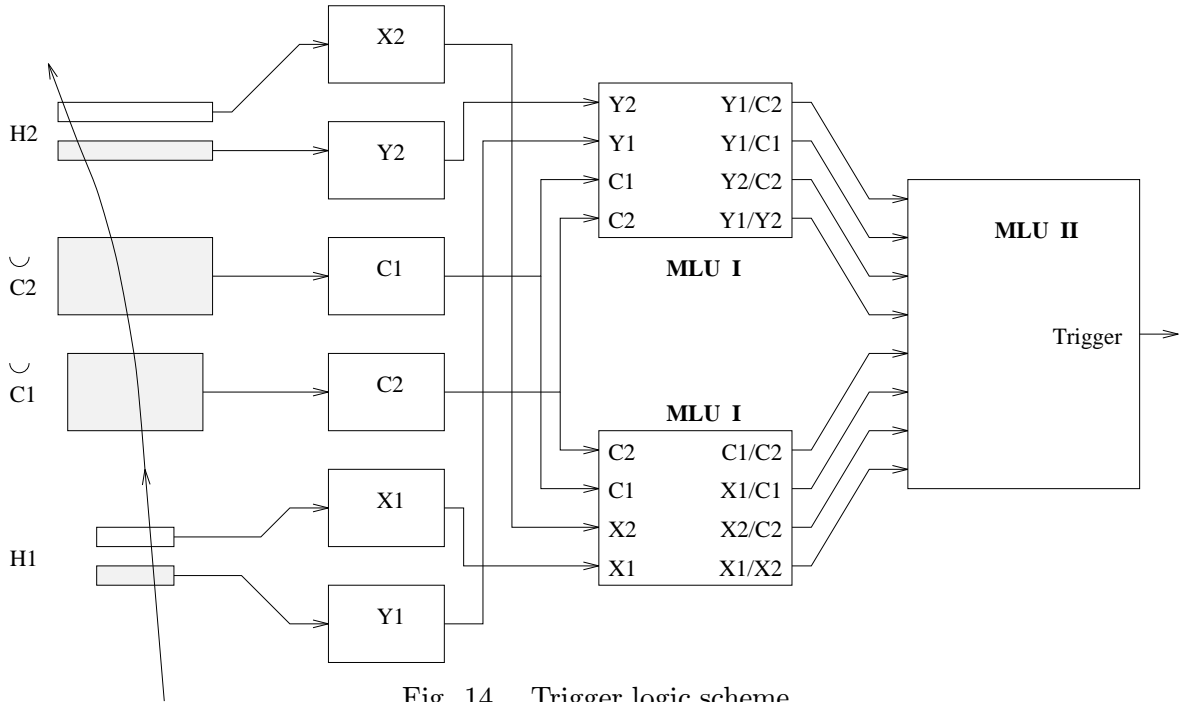


Fig. 14. Trigger logic scheme.

The information from each trigger hodoscope and Čerenkov counter comes to the multitrack discriminator-coders. One part of the programmable logic forms correlation signals between the Čerenkov counters and X-coordinates, the second part – between Čerenkov counters and Y-coordinates. Eight pair correlations come to the logic analysis module, where tracks are separated according to type and transverse momentum. Multichannel Čerenkov counters allow removal of false combinations for pions and reduce significantly false combinations for kaons. It simplifies the event selection in transverse momentum with threshold $1 \div 1.5 \text{ GeV}/c$ and allows setting of the trigger rate at the level of $1000 \div 2000$ events per accelerator spill. While measuring the momentum, thresholds will be optimized for each type of particle.

One charged-particle trigger has been prepared and tested. Work on the multi-particle trigger is in progress.

Triggering with hadron calorimeter. Analog information (18 columns each with 12 elements) is read out from the hadron calorimeter to form the first level trigger. In each column, the signals from 12 counters are summed and also attenuated proportionally to $\sin\theta_x$. The signal $E_x = \sum E_i \cdot \sin\theta_{x_i}$ is proportional to the transverse momentum p_T , and it can be used to cut on the particles with small p_T .

The total cross-section of the charged hadrons hitting the hadron calorimeter is around 0.75 mb, when the experimental setup makes an angle 9° with the beam line. Fig. 15 presents the differential cross section $d\sigma/dp_T$ of the charged hadrons without and with various E_x cuts : 0.5, 1.0, 1.5 and 2.0 GeV/c. These cuts reduce the information flow by factors of 4, 93, 1800 and 17000 respectively.

As it follows from the estimations, the usage of the trigger with the cut $E_x \geq 1$ GeV/c allows a reduction of the data flow to 400 events per accelerator cycle, from an event rate of $3.5 \cdot 10^4$ events per cycle in the hadron calorimeter.

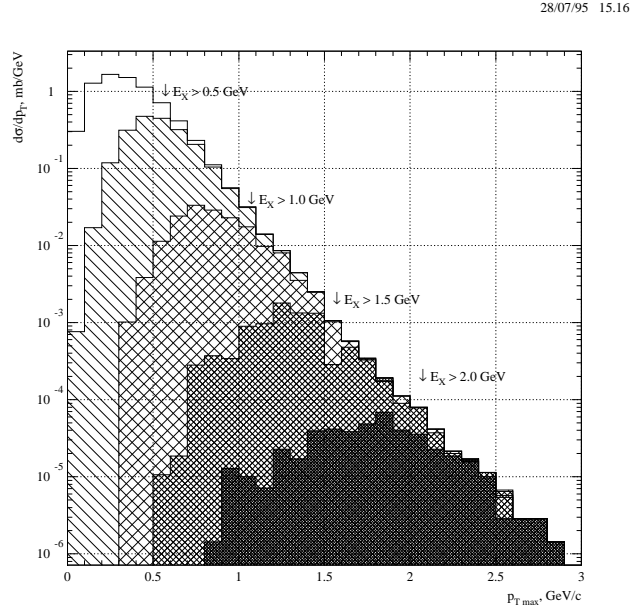


Fig. 15. Triggering with the hadron calorimeter.

7. Estimates of cross sections and uncertainties

To simulate the physical processes, event generators PYTHIA [PYT92] and ISAJET [ISA86] were used.

Acceptance of the setup. Two-dimensional distributions are shown in fig. 16 presenting the total acceptance for charged pions and kaons. Partial acceptances corresponding to chosen angles between the beam line and the setup axis cover a certain part of the dashed region. The calculations have been performed for the Čerenkov counters Č1 and Č2 filled with freon and nitrogen, respectively.

The accessible region of x_F depend on p_T values. The maximum value of x_F in the forward direction is 0.6 at

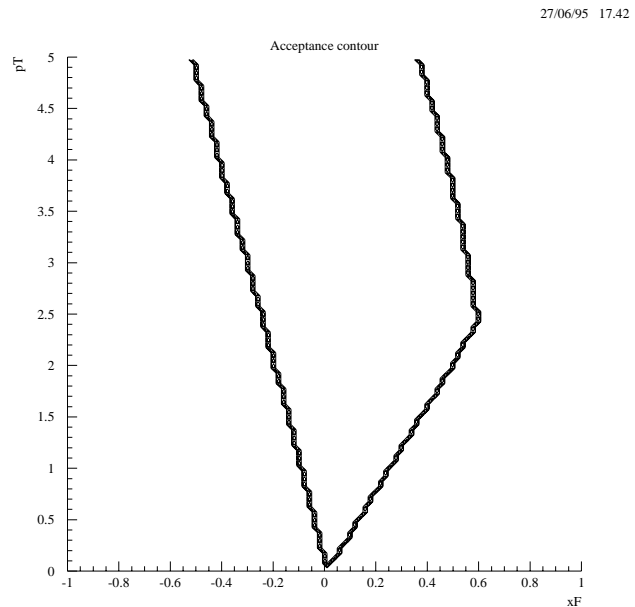


Fig. 16. Acceptance of the experimental setup for π^\pm, K^\pm .

$p_T=2.5$ GeV/c. In the backward region the x_F acceptance is smaller and at the same p_T value it is cut by $x_F=-0.25$.

At small x_F the range of p_T values cover the full kinematics region and can be limited only by statistics.

Inclusive production of π^\pm , K^\pm , p and \bar{p} . Fig. 17 presents the Monte Carlo calculations of the acceptance for the charged particles identified with the counters Č1 and Č2. These particles are detected in the kinematic region determined by the rapidity $-0.4 < y < 1$ and the transverse momentum $0.5 < p_T < 3$ GeV/c with the average efficiency 0.13. The maximum detection efficiency for any type of charged particles is roughly 0.2. This value is achieved approximately at the same rapidity, $y=0.5$ for pions, kaons and protons. For kaons and protons, the maximum detection efficiency is obtained in the region of the transverse momenta $p_T=1.5-2.0$ GeV/c. For the charged pions, the calculated efficiency is maximum at low p_T whereas the low- p_T region is ineffective for heavier charged particles.

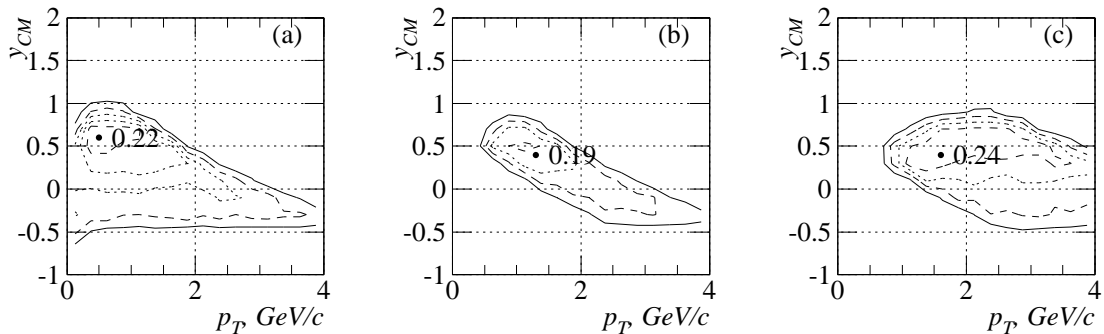


Fig. 17. The spectrometer acceptance for π^\pm (a), K^\pm (b), p and \bar{p} (c) versus p_T and y . The fat points and accompanying values mark the positions of the efficiency maximum and its value, respectively. The topographic lines are drawn in steps of 0.04.

To estimate the hard production cross sections of the charged pions, kaons and protons in pp interactions at 70 GeV/c, we used the experimental data obtained in IHEP at FODS [ABR81]. The invariant production cross sections $Ed^3\sigma/dp^3$ at $\theta^* = 90^\circ$ measured at FODS are shown in fig. 18. Having normalized the Monte Carlo output to these experimental cross section we were able to get the particle fluxes in the acceptance of the spectrometer.

In Table 1 we present the cross section for detected π^\pm , K^\pm , p and \bar{p} , the expected number of events during the 30-day accelerator run with the luminosity $\mathcal{L} = 1 \cdot 10^{30} \text{cm}^{-2} \text{s}^{-1}$.

Table 1. Expected yields and accuracies in the asymmetry measurements in π^\pm , K^\pm , p and \bar{p} production in various p_T intervals for a 30-day accelerator run with the luminosity $\mathcal{L} = 10^{30} \text{cm}^{-2} \text{s}^{-1}$.

p_T , GeV/c	particle	σ_{det} , mb	N_{det} per 30 days	stat. error δA_N
1.0 – 1.5	π^+	$5.1 \cdot 10^{-2}$	$1.3 \cdot 10^8$	0.001
1.5 – 2.0		$4.9 \cdot 10^{-3}$	$1.3 \cdot 10^7$	0.003
2.0 – 2.5		$4.3 \cdot 10^{-4}$	$1.1 \cdot 10^6$	0.011
2.5 – 3.0		$3.6 \cdot 10^{-5}$	$9.4 \cdot 10^4$	0.038
1.0 – 1.5	π^-	$3.5 \cdot 10^{-2}$	$9.2 \cdot 10^7$	0.001
1.5 – 2.0		$3.5 \cdot 10^{-3}$	$9.1 \cdot 10^6$	0.004
2.0 – 2.5		$2.9 \cdot 10^{-4}$	$7.4 \cdot 10^5$	0.015
2.5 – 3.0		$2.1 \cdot 10^{-5}$	$5.5 \cdot 10^4$	0.053
1.0 – 1.5	K^+	$1.1 \cdot 10^{-2}$	$3.0 \cdot 10^7$	0.002
1.5 – 2.0		$1.4 \cdot 10^{-3}$	$3.6 \cdot 10^6$	0.007
2.0 – 2.5		$1.4 \cdot 10^{-4}$	$3.6 \cdot 10^5$	0.021
2.5 – 3.0		$1.2 \cdot 10^{-5}$	$3.2 \cdot 10^4$	0.070
1.0 – 1.5	K^-	$3.6 \cdot 10^{-3}$	$9.2 \cdot 10^6$	0.004
1.5 – 2.0		$4.5 \cdot 10^{-4}$	$1.2 \cdot 10^6$	0.011
2.0 – 2.5		$3.9 \cdot 10^{-5}$	$1.0 \cdot 10^5$	0.040
2.5 – 3.0		$2.8 \cdot 10^{-6}$	$7.1 \cdot 10^3$	0.150
1.0 – 1.5	p	$3.7 \cdot 10^{-2}$	$9.5 \cdot 10^7$	0.001
1.5 – 2.0		$4.6 \cdot 10^{-3}$	$1.2 \cdot 10^7$	0.004
2.0 – 2.5		$5.3 \cdot 10^{-4}$	$1.4 \cdot 10^6$	0.011
2.5 – 3.0		$5.7 \cdot 10^{-5}$	$1.5 \cdot 10^5$	0.032
1.0 – 1.5	\bar{p}	$1.5 \cdot 10^{-3}$	$3.8 \cdot 10^6$	0.006
1.5 – 2.0		$1.4 \cdot 10^{-4}$	$3.6 \cdot 10^5$	0.021
2.0 – 2.5		$9.7 \cdot 10^{-6}$	$2.5 \cdot 10^4$	0.079

Inclusive π^0 production. Neutral pions are detected with the electromagnetic calorimeters EC1 and EC2. For angles between the beam line and main spectrometer arm of 80 mrad (position 1) and 157 mrad (position 2), the π^0 detection efficiency reaches 40% and 10% respectively, as is seen in fig. 19. If π^0 's are produced in cms backward hemisphere (300 mrad, position 3) the geometrical efficiency ranges from 1 to 3% at $x_F = -0.2 \div -0.4$.

This figure shows also the two-dimensional distributions for π^0 fluxes in the 100-shift accelerator run for the three angle positions of the calorimeter EC1.

Inclusive production of K_S^0 , $\phi(1020)$ and Λ . The unstable hadrons will be detected in the dominant decay channels

$$K_S^0 \rightarrow \pi^+\pi^-, \quad \phi \rightarrow K^+K^-, \quad \Lambda \rightarrow p\pi^-,$$

with the decay probabilities 68.6%, 49.1% 64.1%, respectively. In estimates of the production cross sections, the experimental data on inclusive production of ϕ [AKE77], K_S^0 and Λ [AMM86] were used. The total production cross sections in pp collisions at 70 GeV/c are equal to

$$\sigma(\phi(1020)) = 0.5 \text{ mb}, \quad \sigma(\Lambda) = 3.4 \text{ mb}, \quad \sigma(K_S^0) = 3.4 \text{ mb}.$$

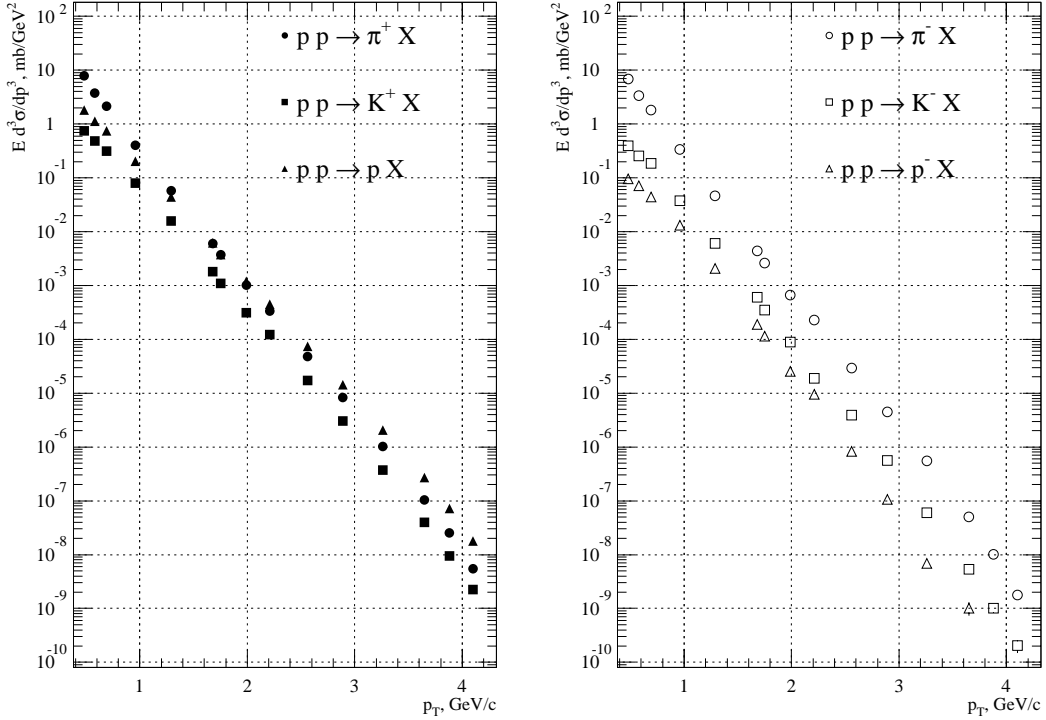


Fig. 18. The invariant cross sections $E d^3 \sigma / dp^3$ at $\theta^* = 90^\circ$ for π^\pm , K^\pm , p and \bar{p} production in pp collisions at 70 GeV/c [ABR81].

As K_S^0 and Λ have sizeable mean life times, it will be reasonable – to reduce the background – to detect only those decay products which originate downstream of the target. The detected spectra of the invariant pair mass $K^+ K^-$, $p\pi^-$ and $\pi^+ \pi^-$ are shown in fig. 6. The detected Λ and K_S^0 have no sizeable background, and under the ϕ peak the background is equal to 18%. The Monte Carlo widths of the reconstructed particles are calculated to be as follows:

$$\phi - 4.5 \text{ MeV}, \quad K_S^0 - 5.6 \text{ MeV}, \quad \Lambda - 1.5 \text{ MeV}.$$

The detected K_S^0 , $\phi(1020)$ cover the kinematical regions shown in fig. 20 versus y and p_T . The threshold Cerenkov counters allow us to detect K_S^0 and $\phi(1020)$ at the transverse momentum $p_T > 0.2 \text{ GeV/c}$, Λ — at $p_T > 0.8 \text{ GeV/c}$.

The Table 2 presents the cross sections of the detected particle and expected numbers of the particles in the 30-day accelerator run at the luminosity $\mathcal{L} \sim 10^{30} \text{ cm}^{-2} \text{ s}^{-1}$.

Table 2. The total cross sections, σ_{det} , and the fluxes N_{det} of the detected particles with strangeness in the 30-days run.

Particle	$\sigma_{det}, \mu\text{b}$	N_{det}
$\phi(1020)$	14	$3.6 \cdot 10^7$
Λ	7.4	$1.9 \cdot 10^7$
K_S^0	22	$5.7 \cdot 10^7$

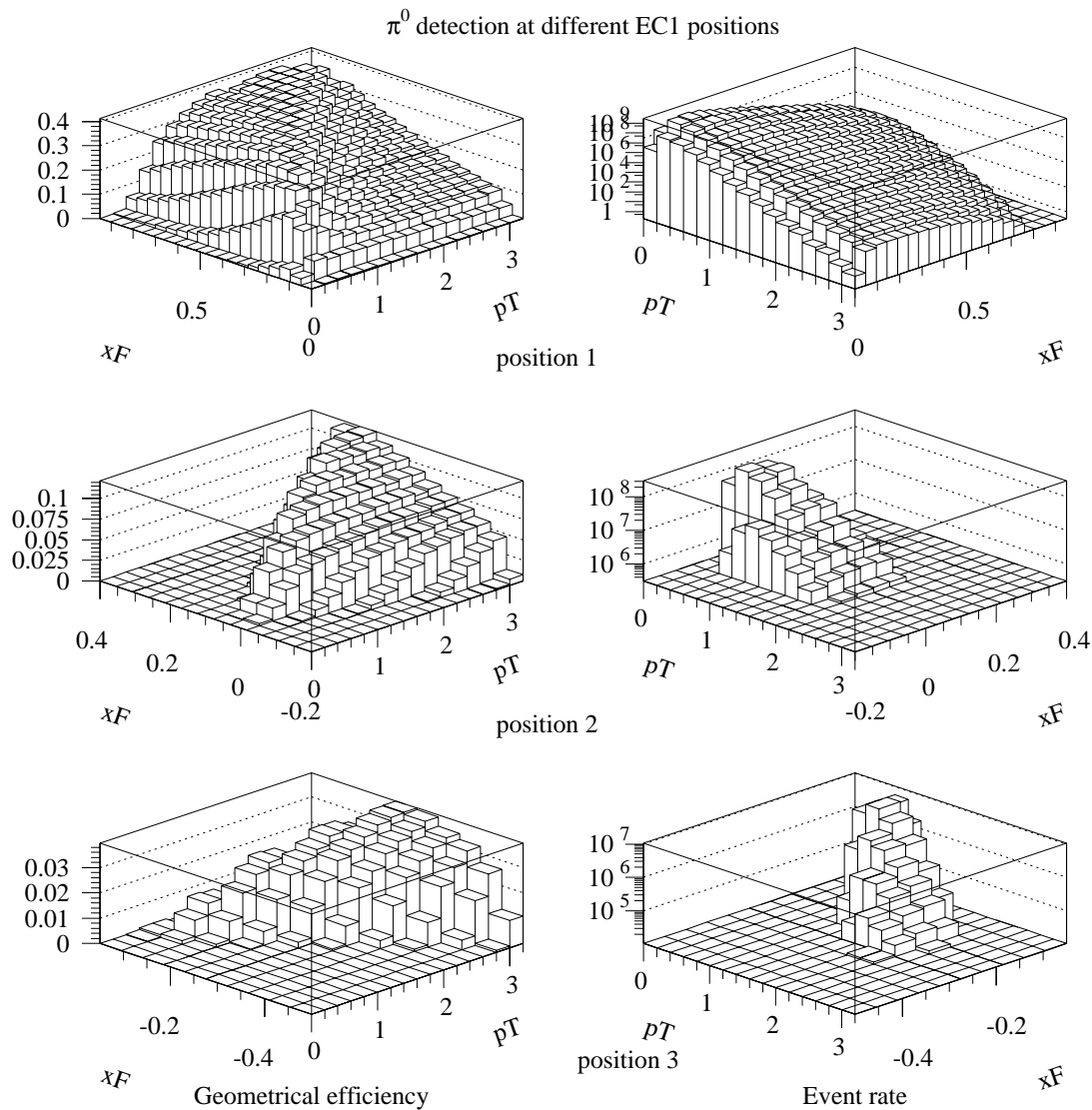


Fig. 19. π^0 detection efficiencies and fluxes in the 100-shift accelerator run for the three angle positions of the main arm of the setup: position 1 - 80 mrad; position 2 - 157 mrad; position 3 - 300 mrad.

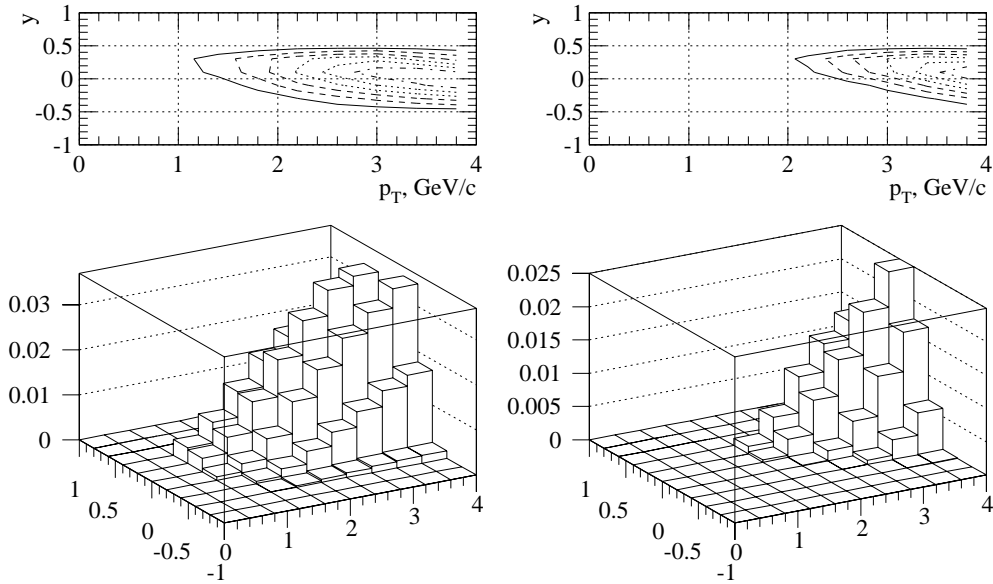


Fig. 20. Detection efficiencies for $\phi(1020)$ and K_S^0 versus p_T and y .

Pion pair production in the region of back-to-back kinematics. In RAMPEX the most sensitive signature of hard parton subprocesses will be detection of two particles, mainly pions, with large transverse momenta in both arms of the setup. This corresponds to particle production at $x_F \sim 0$ in cms with the large opposite transverse momenta (back-to-back kinematics). In fig. 21 the differential cross sections are presented for the detected pairs $\pi^+\pi^0$ with back-to-back kinematics.

Although it is difficult to select these events due to the small cross section and ambiguity problems, they are very interesting because they can be related phenomenologically to the twist-2 chiral-odd quark distribution $h_1(x)$.

Statistical errors in A_N measurements. The absolute statistical error δA_N in the asymmetry measurement is defined as

$$\delta A_N = \frac{D(1+B)}{P} \frac{1}{\sqrt{n}}. \quad (9)$$

This expression includes the dilution factor D , the ratio B of the background to signal, the target polarization P and the number of events n . The dilution factor D depends on the kinematics, and its p_T -dependence can be evaluated using the FODS experimental data on the A -dependence of the differential cross sections [ABR80].

To reach the reasonable values of the asymmetry uncertainties in most reactions under study, we need about 600 U-70 shifts. In Table 1 the expected inaccuracies in some A_N measurements are presented.

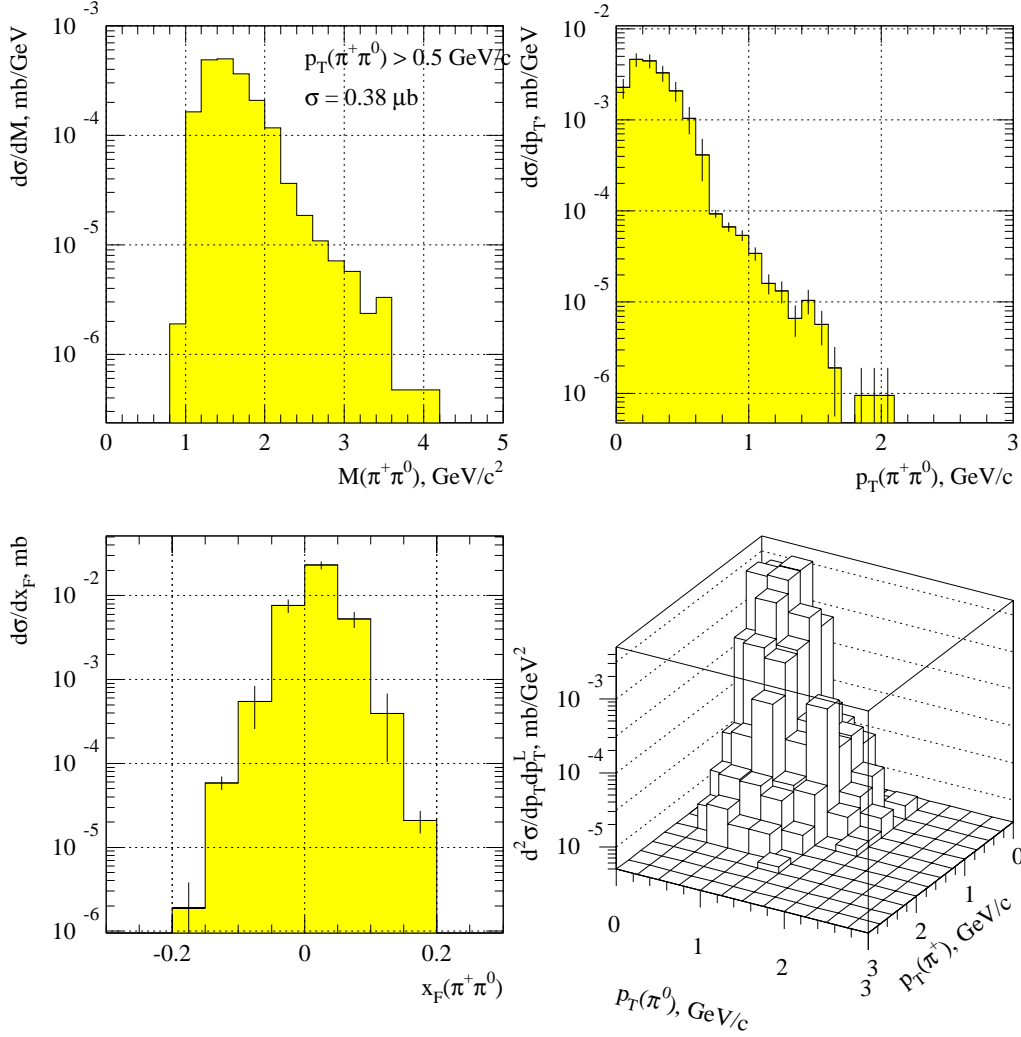


Fig. 21. Differential distributions of the $\pi^+\pi^0$ pair production in the back-to-back kinematics.

8. Status of equipment

The experimental setup is being constructed as a rather universal and flexible one for fixed-target experiments. It allows reasonable detection of charged and neutral particles and, if necessary, strong change of kinematic region of measurements. Two arms provide various possibilities to measure produced particles in the opposite cms hemispheres.

8.1. Acceptance

As the magnet aperture (240 mrad) is much bigger than the the detectors' acceptance (120 mrad) downstream of the magnet, the main spectrometer arm can move – within the magnet acceptance – in zx -plane to cover x_F -range from -0.5 to 0.5 for charged hadrons and from -0.5 to 0.9 for neutral mesons with $p_T < 3$ GeV/c without getting out of the magnet aperture.

8.2. Composition of the equipment

The whole setup configuration is divided into two parts - the basic version and the auxiliary detector. **The basic configuration** includes the following detectors:

- the beam equipment consisting of three trigger counters, three threshold Čerenkov counters (to be used with the π^- beam) and two hodoscopes to measure the coordinates of beam particle;
- the polarized target;
- the spectrometer made of magnet and five blocks of MWPC(9000 channels);
- two multichannel threshold Čerenkov counters (24 channels);
- electromagnetic sandwich (lead-scintillator) calorimeter made of 60 supermodules with cell $38 \times 38 \text{ mm}^2$ and 36 supermodules with cell $76 \times 76 \text{ mm}^2$ (1104 channels in total);
- compensated hadron sandwich (lead-scintillator) calorimeter (216 channels);
- front-end electronics;
- data acquisition system;

The auxiliary detector to study back-to-back kinematics in production of neutral mesons includes:

- fine cell gamma detector made of PbWO_4 crystals;

8.3. Equipment production and tuning

Beam diagnostics. We intend to use the existing beam detectors which are now used for the PROZA setup at the channel 14.

Polarized target. At the moment we consider two options. We have the polarized proton propane-diol target which works for the PROZA. Another option is the University of Michigan ammonia target. It has much better performance (higher polarization and smaller dilution factor). This options are under discussion and decision will be taken soon.

Spectrometer. The spectrometer magnet was built for the NEPTUN experiment at the UNK by the JINR team; they also built a set of MWPCs (12000 channels in total). At present the magnet is installed in channel 14 and has been successfully powered. Measurement of the field map is scheduled for one of the forthcoming U-70 run. Five sets of MWPC's, together with front-end electronics, have been shipped to IHEP after preliminary tests and tuning at JINR. Minor modifications to the stand design are needed to install them. Some work is needed for cabelling. These MWPC's could be installed in the Fall of 1997.

Čerenkov counters. Both counters are in place at the channel 14 and they are subject to modifications. The modifications consist of redesign of the PM support (which is completed at the moment) and new mirror surface finish (to be done at the estimated price of \$40 per mirror) for more effective reflection in the short wave length part of

spectrum. We already have 28 large-cathode photomultipliers in hand. We hope to have both counters ready for tests and tuning by the Fall of 1997.

Electromagnetic calorimeter. EMC1 was built for the NEPTUN project and tested in beam. It is sandwich type calorimeter made of 3 mm lead and 5 mm scintillator plates with lateral dimensions 38x38 mm². As of August 1997 we have 84 supermodules in total, and 40 supermodules have been tested. High voltage supplies were tested and now they are ready to be used. A state-of-the-art thermostabilized monitoring system was designed and passed extensive tests both on the bench and in beam, and demonstrated excellent performance, with very low drift in time and temperature.

Hadron calorimeter. The compensating hadron calorimeter developed for NEPTUN experiment has been successfully tested in a variety of particle beams and it demonstrated the very high resolution and long term stability. At the moment we have 300 modules which are to be assembled. The whole detector could be ready for beam tests in the fall of 1997.

Front-end and trigger electronics. The electronics for beam diagnostics, trigger hodoscopes, Čerenkov counters and MWPCs are in hand and ready to use. The first shipment of ADC modules and crates (5 crates×320 channels) is expected in mid 1997 while the rest (1 crate) will be ready in Fall 1997.

DAQ. The data acquisition system prototype based on the MC68020 microprocessor and the OS9 platform in VME crates has been tested. By the Fall of 1997 missing VME blocks and custom MISS blocks will be shipped and incorporated in the DAQ.

Fine cell gamma detector. Together with other groups in our institute, we have developed a state-of-the-art electromagnetic calorimeter which is made of PbWO crystals and has numerous excellent features such as radiation hardness, fast response time, high density and very high resolution. A prototype of this calorimeter has been tested in laboratories all around the world. The full scale detector production is under way and could be completed in 1998. Due to the high price of the PbWO crystals we have joined efforts of different groups and anticipate the shared use of this detector for different experiments in our institute.

9. What shall we study – short formulation

In the previous sections we have discussed the inclusive reactions which will be studied in RAMPEX. In principle the chiral-odd structure functions can be studied in $p_{\uparrow}p_{\uparrow}$ or $p_{\rightarrow}p_{\uparrow}$ through the real photon or virtual photon (Drell-Yan pair) production.

This method has an advantage of exact knowledge of the integrand in theoretical expression for A_N . The problem is that the h functions are convoluted with other quark spin distributions which are unknown or measured with sizeable experimental errors.

An advantage of hadron experiments with one polarized initial proton is a possible isolation of h functions in appropriate phenomenology because no other spin-dependent

distributions are needed. However the problem with this approach is the current ambiguity of the twist-3 phenomenology in different models.

Thus each class of reactions possesses internal advantages and disadvantages, and the proposed one-spin experiment with hadron production should supply high energy spin physics with unique data.

In fig. 22 we display the compressed information about the RAMPEX studies: types of reactions, kinematic regions and theoretical topics to be tested. Some cells in the chart are marked with $h_1(x)$ and $h_L(x)$ to show where the models (may) include the chiral-odd spin distributions.

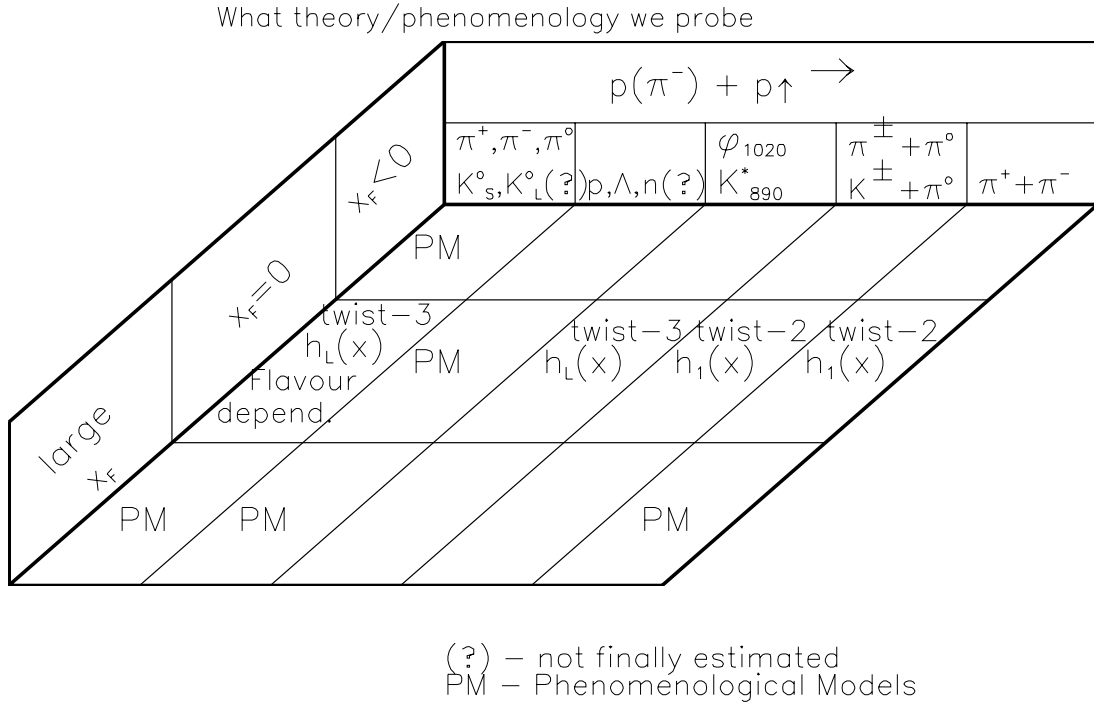


Fig. 22. Short layout of the RAMPEX studies.

References

- [ABR80] V.Abramov et al., Yad. Fiz. (Soviet J. Nucl. Phys.) 31 (1980) 660.
- [ABR81] V.Abramov et al., Yad. Fiz. (Soviet J. Nucl. Phys.) 31 (1980) 937; Pis'ma v Zhetf (Lett. to Sov. J. Exp. and Theor. Phys.) 33(1981) 304.
- [ADA91a] D.L.Adams et al., Phys. Lett. B264(1991)462 (π^\pm at large x_F , 200 GeV/c);
D.L.Adams et al., Z.Phys. C56(1992)181 (π^0 at large x_F , 200 GeV/c).
- [ADA91b] D.L.Adams et al., Phys.Lett. B276(1991)531 (π^0 at $x_F=0$).

- [ADA94] D.Adams et al., Preprint CERN-PRE/94-116, July 1994
Phys. Lett. B336(1994)125 ($e_{\rightarrow} + p_{\uparrow}$).
- [ALE92] G.Alekseev et al., A study of characteristics of compensating lead hadron calorimeter, Preprint IHEP 92-36, 1992.
- [ALE94] A.M.Aleev et al., A threshold gaseous 32-channel Čerenkov counter at the spectrometer EXCHARM, Preprint JINR P13-94-520, Dubna, 1994.
- [AMM76] V.V.Ammosov et al., Nucl.Phys. B115(1976)269.
- [AMM86] V.V.Ammosov et al., Z.Phys. C30(1986)175.
- [ANS95] M.Anselmino, M.Boglione, F.Murgia Phys. Lett. B362(1995)164.
- [ANS96] M.Anselmino and F.Murgia, private communication.
- [AKE77] C. W. Akerlof et al.. Phys. Rev. Lett. 1977, vol. 39 861;
Daum et al. Nucl. Phys. 1981, vol. B186 205;
Dijkstra et al. Zeitsch. für Phys. 1986, vol. C31 375;
M. Aguilar-Benitez et al. CERN-PPE-91-21;
Yu. Antipov. Phys. Lett. 1982, vol. 110B 326;
D. Drijard et al. CERN/EP 81-12.
- [APO90] V.D.Apokin et al., Phys. Lett. B243(1990)461. (π^0 at $x_F = 0$, 40 GeV/c).
- [ARE96] a) Yu. Arestov, Summary of the RAMPEX Round Table. In Proc. 12th Int. Symp. on High Energy Spin Physics, Amsterdam, Sept. 1996. Edited by C.W. de Jager, T.J. Ketel, P.J. Mulders, J.E.J. Oberski and M. Oskam-Tamboezer.
b) Yu. Arestov, Twist-3 induced asymmetries in hard production at 70 GeV/c, *ibid.*
- [ARE97] Yu. Arestov, RAMPEX - a new spin experiment, NIM A275 (in press).
- [ART90] X.Artru and M.Mekhfi, Z.Phys. C45(1990)669;
X.Artru, Proposal for measuring transversity distributions in DIS, LYCEN/9353, Oct. 1993.
- [ART94] X. Artru, J.Czyzewski, H.Yabuki, LYCEN/9423, TPJU 12/94, May 1994.
- [ASE93] A. A. Aseev et al. Nucl. Instr. Meth. A330 (1993) 39.
- [BON90] B.E.Bonner et al., Phys. Rev. D41(1990)13.
- [BOR76] N.S.Borisov, E.I.Bunyatova and Yu.F.Kiselev, JINR preprint 13-10253, Dubna, 1976; JINR preprint 13-10257, Dubna, 1976.
- [BOR95] C.Boros, Z.Liang and T.Meng, Phys Rev D51(1995)4867
and refs therein.

- [BRO80] S. J. Brodsky, G. P. Lepage. Phys. Rev. D22 (1980)2157.
- [BRU75] K. Bruneton et al., Preprint IHEP 75-79; PTE (Sov. J. Devices and Exp. Technics 5(1976)46; Nucl. Instr. Meth. 125(1975)585; I. Avvakumov et al., Preprint IHEP 81-15, 1981.
- [BUY94] O.V. Buyanov, R. Chipaux, A.A. Fyodorov et al. A first electromagnetic calorimeter prototype of $PbWO_4$ crystals, Nucl. Instr. Meth. A 349 (1994) 62-69.
- [COL93] J. C. Collins, Nucl. Phys. B396(1993)161.
- [COL94] J.C. Collins, S.F. Hoppelman and G.A. Ladinsky, Preprint PSU/TH/101, May 1993; Nucl. Phys. B420(1994)565.
- [COL96] J.C. Collins and G.A. Ladinsky, On $\pi - \pi$ Correlations in Polarized Quark Fragmentation Using the Linear Sigma Model, Preprint PSU/TH/114, Feb. 1996.
- [DIC75] L. Dick et al., Phys. Lett. B57(1975)93 ($\pi^\pm p_\uparrow \rightarrow \pi^\pm + X$ at 8 GeV/c).
- [DIS94] A. Thomas, Review of the spin crisis, Int. Symp. on High Energy Spin Physics, Bloomington, Sept. 1994.
- [DOR91] A.F. Dorokhov, N.I. Kochelev, Phys. Lett. B259(1991)335.
- [EFR82] A.V. Efremov and O.V. Teryaev, Sov. J. Nucl. Phys. 36(1982)140.
- [EFR84] A.V. Efremov and O.V. Teryaev, Sov. J. Nucl. Phys. 39(1984)962; Yad. Fiz. 39(1984)1517.
- [EFR85] A.V. Efremov and O.V. Teryaev, Phys Lett 150B(1985)383; see also [ADA94] concerning asymmetry A_{LT} depending on both twist-3 structure functions g_T and h_L in lepton pair production.
- [EFR92] A.V. Efremov, L. Mankiewicz and N.A. Törnqvist, Phys. Lett. B284(1992)394.
- [EFR95] A.V. Efremov, V.M. Korotkiyan and O.V. Teryaev, Phys. Lett. B348(1995)577.
- [EKT95] A.V. Efremov, V.M. Korotkiyan and O.V. Teryaev, Phys. Rep. 261(1999) N1,2.
- [EXPAN] R. Klem et al., Phys. Rev. Lett. 36(1976)929 ($p_\uparrow + p \rightarrow \pi^\pm + X$ at 6 and 12 GeV/c);
W.H. Dragoset et al., Phys. Rev. D18(1978)3939 ($p_\uparrow + p, p_\uparrow + d \rightarrow \pi^\pm, K^\pm, p + X$ at 11.75 GeV/c);
J. Antille et al., Phys. Lett. B94(1980)523 ($p + p_\uparrow \rightarrow \pi^\circ + X$ at 24 GeV/c);
B.E. Bonner et al., Phys. Rev. Lett. 58(1987)447; Phys. Rev. D38(1988)729 ();
B.E. Bonner et al., Phys. Rev. Lett. 61(1988)1918 (π°).

- [GOL89] G.R.Goldstein and M.J.Moravcsik, Ann.Phys. (N.Y.) **98**,128(1976);
142,219(1982);**195**,213(1989).
- [ISA86] F.E.Paige, S.D.Protopopescu, in 'Physics of the Superconducting SuperCollider
1986', p.320.
- [JAF91] R.L. Jaffe and X.Ji, Phys.Rev.Lett. 67(1991)552.
- [JIX92] X.-D. Ji, Phys.Lett. B284(1992)137.
- [LEA93] E.Leader and K.Sridhar, Phys Lett B311(1993)324.
- [NAC77] O.Nachtmann, Nucl Phys B127(1977)314.
- [PEN95] A.Penzo, E-704 results on spin effects in Λ inclusive production..., Proc. 2nd
Meeting 'Possible Measurements of Singly Polarized pp_{\uparrow} and pn_{\uparrow} Collisions at HERA',
Zeuthen, Aug. 31 - Sept. 1, 1995.
- [PEN90] J.Qiu and G.Sterman, Nucl Phys B353(1991)105; also in Proc.
of Polarized Collider Workshop, University Park, Pennsylvania,1990.
- [PYT92] T.Sjöstrand. Pythia 5.6 and Jetset 7.3, physics and manual. CERN-
TH.6499/92
- [QIS91] J.Qiu and G.Sterman, Nucl.Phys. B353(1991)137.
- [QST91] J.Qiu and G.Sterman, Phys.Rev.Let. 67(1991)2264;
- [RAL79] J.P.Ralston and D.E.Soper, Nucl.Phys. B152(1979)109.
- [RSC92] RSC Collab.- R.Carlitz,J.Collins,S.Heppelman and R.Jaffe,
Measuring transversity densities in singly polarized hadron-hadron collisions. (Note
for RHIC Spin Coll.).
- [RYS90] M.G. Ryskin, Yad Fiz (Soviet Journal of Nuclear Physics)48(1988)1119.
- [SAR90] S.Saroff et al., Phys. Rev. Lett. 64(1990)995. (π^{\pm} at $x_F = 0, 13, 18$ GeV/c).
- [SIV90] D.Sivers, Phys. Rev. D41(1990)83; and also in Phys.Rev. D41(1991)261.
- [TRO95] S.M.Troshin and N.E.Tyurin, Spin Content of Constituent Quarks and One-
spin Asymmetries in Inclusive Processes, Preprint IHEP 95-40, Protvino 1995;
S.M.Troshin and N.E.Tyurin, On asymmetry in inclusive pion production, Preprint
IHEP 95-146, Dec.1995; S.M.Troshin and N.E.Tyurin, Phys Rev D52(1995)3862.

Received September 18, 1997

10. Appendix A: Parton densities in a polarized nucleon

Intrinsic non-perturbative hadron structure is described in terms of quark parton distributions. There are 9 quark distribution functions: three at each twist n , $n=2,3,4$ which are specified as the twist- n spin-average distribution, the twist- n spin distribution and the twist- n 'spin-dependent' distribution [JAF91].

The well known functions $g_i(x)$, chiral-even quark distributions in the polarized proton, are related to the proton matrix element of bilinear quark operators as follows:

$$\langle pS | \bar{q} \gamma_\mu \gamma_5 q | pS \rangle = \{g_1(x); g_2(x); g_3(x)\}.$$

Here the brackets denote the corresponding vector or tensor structures of vectors p_μ, s_μ, n_μ (gauge vector) which contain the functions $g_i(x)$ as coefficients. The function g_1 relates to twist-2 and g_2 includes, beside twist-3 contributions, a partial contribution of operators which define g_1 . The latter contribution is dropped in the sum $g_T(x) = g_1(x) + g_2(x)$ actually relating to twist-3. The structure functions $g_1(x)$ and $g_T(x)$ sense the quark spin densities in longitudinally and transversely polarized proton, respectively. (see also review [EKT95]).

Likewise the functions $h_i(x)$, the spin-dependent chiral-odd quark distributions, appear in the matrix element

$$\langle pS | \bar{q} \sigma_{\mu\nu} i\gamma_5 q | pS \rangle = \{h_1(x); h_2(x); h_3(x)\}.$$

Here $h_1(x)$ corresponds to twist-2 terms and a combination of functions h_1 and h_2 taken in the form $h_L(x) = h_2(x) + h_1(x)/2$ includes the twist-3 contribution only. The structure functions h_1 and h_L are now a subject of common interest in the theory of spin phenomena.

Although $h_1(x)$ is the twist-2 structure function it cannot be interpreted as easily as $g_1(x)$. The transverse spin operator is regarded as a 'bad' operator which depends on dynamics. Nevertheless there is a 'transversity' basis in hadron interactions where the density h_1 expresses clearly a proton property called transversity, so the twist-2 structure function $h_1(x)$ is called *transversity* distribution. It does not coincide with the distribution of quarks with transverse spins (g_T). In this sense the new function h_1 is more understandable than g_T , the twist-3 distribution, which is sensitive to quark-gluon correlations.

The terms 'transversity distribution' (h_1) and 'transverse spin distribution' (g_T) are different.

h_L , the linear combination of h_1 and h_2 , is a pure twist-3 distribution. It also can not be interpreted as a simple quark distribution because it expresses a property connected with the quark-gluon dynamics of confinement.

The role and usage of these structure functions can be understood by studying the production of the Drell-Yan pairs in collisions of polarized protons. The double-spin asymmetries are proportional to bilinear combinations of the structure functions g_i and h_i (references to original papers can be found in [JAF91]).

$$\begin{aligned} p \rightarrow p \rightarrow &\rightarrow \ell^+ \ell^- + X : & A_{LL} &\sim g_1 g_1 \\ p \uparrow p \uparrow &\rightarrow \ell^+ \ell^- + X : & A_{TT} &\sim h_1 h_1 \\ p \rightarrow p \uparrow &\rightarrow \ell^+ \ell^- + X : & A_{LT} &\sim (g_1 g_T - h_L h_1). \end{aligned}$$

As is seen, the asymmetries which are fully determined by the twist-2 structure functions appear when colliding protons both polarized either longitudinally or transversely. The twist-3 structure

functions contribute as a convolution twist-2 \otimes twist-3 when the protons are polarized differently, one longitudinally and the second transversely.

The twist-3 structure function $g_T(x)$ was extracted from the double-spin asymmetry in deep inelastic scattering of longitudinally polarized electrons on transversely polarized protons $e_{\downarrow} + p_{\uparrow}$ (see ref. [ADA94]).

From experimental data on one-spin asymmetries, no information on the twist-3 chiral-odd distributions has been obtained so far.

11. Appendix B: Factorization theorem with one spin

A study of hard processes is based on the factorization hypothesis which was initially formulated for the leading twist contributions. The expression contains the twist-2 factors, and it is applicable to hadron reactions both with averaged spins and with two known spins (two initial polarized particles or one initial polarized particle and one final polarized particle) [BRO80]:

$$\sigma = H_o \otimes f_2 \otimes f_2 \otimes D_2. \quad (10)$$

Here H_o denotes the so-called coefficient functions of the hard subprocess, and f_n, D_n are non-perturbative hadron matrix elements of twist- n .

The factorization formula for a hard process with one polarized particle cannot be deduced from (10) as that for a hard process with two polarized hadrons. The problem of infra-red stability of isolated factors in expressions of type (10) is more subtle for one polarized particle. Some estimations for corrections of order $\sim 1/Q$ in cross section $\sigma_{\uparrow}(Q)$ were made in refs. [PEN90]. A factorization formula which is based on these papers has the form

$$\sigma_{\uparrow}(Q) = H^o \otimes f_2 \otimes f_2 \otimes D_2 + \frac{1}{Q} H^1 \otimes (f_2 \otimes f_3 \otimes D_2 + f_2 \otimes f_2 \otimes D_3) + O\left(\frac{1}{Q^2}\right). \quad (11)$$

Notations are the same as in (10). The twist-3 terms depend on the transverse polarization of initial hadron.

An explicit factorization formula with the quark spin density matrix ρ_{ij} inside a polarized proton was introduced in ref. [COL94]. It was explored in ref. [ANS95] to predict the x_F -dependence of one-spin asymmetries in hadron interactions.

С.Акименко и др.

Изучение односпиновых асимметрий в pp_{\uparrow}^{-} и $\pi^{-}p_{\uparrow}^{-}$ -взаимодействиях при 70 и 40 ГэВ/с. (Предложение эксперимента).

Оригинал-макет подготовлен с помощью системы \LaTeX .

Ответственный за выпуск Ю.И.Арестов.

Подписано к печати 25.09.97. Формат $60 \times 84/8$.

Офсетная печать. Печ.л. 4.87. Уч.-изд.л. 3.74. Тираж 200. Заказ 1112.

Индекс 3649. ЛР №020498 17.04.97.

ГНЦ РФ Институт физики высоких энергий
142284, Протвино Московской обл.

